Transactions of the I·R·E

Professional Group on Antennas and Propagation

VOLUME AP-2 NUMBER 3 JULY 1954
Published Quarterly

The Institute of Radio Engineers

TRANSACTIONS OF THE I•R•E® PGAP IS A QUARTERLY PUBLICATION DEVOTED TO EXPERIMENTAL AND THEORETICAL PAPERS ON ANTENNAS AND WIRELESS PROPAGATION OF ELECTROMAGNETIC WAVES

MANUSCRIPTS should be submitted to John B. Smyth, Editor, U. S. Navy Electronics Laboratory, San Diego, California. Manuscripts should be original typewritten copy, double spaced, plus one carbon copy. References should appear as footnotes and include author's name, title, journal, volume, initial and final page numbers, and date. Each paper must have an abstract of not more than 200 words. News items concerning PGAP members and group activities should be sent to the News Editor, Mr. H. A. Finke, Polytechnic Research and Development Company, 55 Johnson Street, Brooklyn, New York.

ILLUSTRATIONS should be submitted as follows: All line drawings (graphs, charts, block diagrams, cutaways, etc.) should be inked uniformly and ready for reproduction. If commercially printed grids are used in graph drawings, author should be sure printer's ink is of a color that will reproduce. All half-tone illustrations (photographs, wash, airbrush, or pencil renderings, etc.) should be clean and ready to reproduce. Photographs should be glossy prints. Call-outs or labels should be marked on a registered tissue overlay, not on the illustration itself. No illustration should be larger than 8 x 10 inches.

Copies can be purchased from
THE INSTITUTE OF RADIO ENGINEERS
1 East 79 St., New York 21, N.Y.

PRICE PER COPY: members of the Professional Group on Antennas and Propagation $1.50; members of the IRE $2.25; nonmembers $4.50.

Entered as second-class matter, at the post office at Menasha, Wisconsin, under the act of August 24, 1912. Acceptance for mailing at a special rate of postage is provided for in the act of February 28, 1925, embodied in Paragraph 4, Section 412, P. L. & R., authorized October 26, 1927.

news and views

Administrative Committee Changes

THE administrative committee of the PGAP met in Washington at the time of the May URSI meeting and unanimously elected Delmer C. Ports as Chairman of the Committee for the coming year. In addition, Dr. H. G. Booker was elected Vice Chairman and Dr. George Sinclair accepted the post of Papers Review Chairman.

The committee passed unanimously a resolution to amend the PGAP constitution and bylaws to provide for the election of the Administrative Committee by all members of PGAP. This is to be accomplished by mailing a ballot to each PGAP member with a list of the four choices of the nominating committee with blank spaces opposite each name to allow for comment. Dr. George Sinclair, Chairman of the Nominating Committee, has submitted the following names:

R. A. Halliwell	R. C. Spencer
V. H. Roman	A. W. Straiton

The above proposed members of the Administrative Committee are being submitted to the membership for election for terms expiring May 31, 1957.

For the information of our membership, the present Administrative Committee is as follows:

Term Expires May 31, 1954

P. S. Carter, Chairman
L. J. Chu, Papers Procurement
R. B. Jacques, Advertising
A. H. Waynick, Junior Past Chairman

Term Expires May 31, 1955

H. G. Booker, Papers Review
J. S. Brown, Chapters
D. C. Ports, Vice-Chairman
J. B. Smythe, Editor

Term Expires May 31, 1956

J. T. Bolljahn—Meetings
H. A. Finke, News & Views
George Sinclair, Senior Past Chairman
H. W. Wells, Past Editor
L. C. Van Atta

With great reluctance, P. H. Smith has resigned as Group Secretary-Treasurer because of the pressure of other work. Chairman P. S. Carter has ruled that the post will remain open for the present until filled by an appointment by the incoming chairman.

The next meeting of PGAP Committee is scheduled tentatively for the Hague, Netherlands, August 23, 1954.

News and Views Committee

In an effort to broaden the coverage of the News and Views section of the PGAP, we have written to a number of people in different geographical areas requesting specific assistance in obtaining material.

Allen Ellis of Stamford Research Institute will provide News and Views coverage for this area. Bob Mattingly at the Whippany Laboratories will serve as local news representative for the area. Mr. Clarence Stewart will serve as the local representative for the Washington area. George Sinclair will provide coverage for Canada. Dr. Van Atta is attempting to designate someone for the Los Angeles area.

There is no doubt that a good news section will serve to bring cohesiveness to our group and it will be appreciated if all members co-operate as much as possible with local representatives.

Browder J. Thompson Memorial Prize Award

Because papers appearing in the PGAP Transactions are eligible for the Browder J. Thompson Memorial Prize Award, we are reprinting the specifications to encourage PGAP members to contribute articles:

This award was established by friends of the late Browder J. Thompson, who gave his life in service to his country while prosecuting technical work with the United States Armed Forces in Italy in 1944. The award is to commemorate his interests in science and his many contributions in the field of radio and electronics. A fund of $4,000, established by his friends, is administered by the IRE. The income from this fund provides the annual award. The purpose of the award and the basis upon which its recipient is chosen are as follows:

Its purpose shall be to stimulate research in the field of radio and electronics and to provide incentive for the careful preparation of papers describing such research. The award shall be made annually by the Board of Directors to the author or joint authors under thirty years of age at date of submission of original manuscript (in case of joint authorship, all authors shall be under thirty years of age at date of submission of original manuscript) for that paper of sound

merit recently published in the Technical Publications of the Institute of Radio Engineers which, in the opinion of the Award Committee of the Institute, constitutes the best combination of technical contribution to the field of radio and electronics and presentation of the subject.

Group Chapters and Chapter News

Los Angeles Chapter. The last meeting of the Group was held on April 13. This meeting was a joint meeting of the PGAP and the Professional Group on Aeronautical and Navigational Electronics. The technical program presented two papers, "Effects of Helicopter Rotor Modulation on VOR Receiver," by Henry Blanchard, Stanford Research Institute, Palo Alto, Calif. and "Drag and Weight Considerations in Airborne Antenna Design," by Robert Twomey, Douglas Aircraft Co., Inc., Santa Monica, Calif.

The next meeting of the Los Angeles Chapter will be held on June 2, 1954, at the Institute of Aeronautical Sciences Building. The election of Officers for the Professional Group Chapter will be held at that meeting. The candidates selected by the Nominating Committee are: Chairmen: S. M. Kerber and W. R. Martin; Vice Chairmen: R. Krausz and R. F. Reese; Secretary: E. Lovick, Jr. and D. L. Margerum. Dr. Jesse Greenstein of the Mount Wilson and Palomer Observatories will present a paper on "Radio Astronomy" at this meeting. This topic should be of interest to the Group since some very interesting antenna problems are connected with radio astronomy work.

A questionnaire was mailed to almost 150 members of the Professional Group in the Los Angeles area and others who had attended previous meetings. Seventy replies were received to date. About 35 people indicated that they would be interested in taking an active part in Professional Group activities. Sixty-five wish to be continued on our mailing list. Fifty-four of those replying indicated that they were members of the Professional Group on Antennas and Propagation. An effort will be made to recruit those interested parties who have not as yet become members of the PGAP, but who are interested in local chapter activities.

Technical papers submitted for presentation at the West Coast Electronics Convention August 25 through 27, 1954, in Los Angeles, are now being reviewed by a committee headed by Dr. M. J. Ehrlich.

J. S. Brown, Chairman of the Chapters Committee, reports that a fourth local chapter is in the process of forming. PGAP needs, however, more local activity and more active people in the sections to carry the responsibilities. His observation is that once a chapter is started it goes along on its own momentum. The Chicago Chapter is a good example.

R. B. Jacques, Advertising Manager of the Transactions and organizer of the recently formed Albuquerque-Los Alamos Chapter at Sandia, reports an average attendance of 12 to 15 at meetings. This group sometimes combines its meetings with a Microwave Theory group. Notices are posted in the company house organ and "Fireside Chats" are organized in private homes.

Mr. Clarence Stewart of Jansky & Bailey, Washington, D. C., is laying the groundwork for a PGAP local in the Washington area. Members are urged to get in touch with him to get the group started.

Transactions

An annual subscription rate is being worked out for the Transactions to permit technical libraries and others interested to subscribe. D. C. Ports is Chairman of a Committee studying this problem. Seven hundred complimentary copies of the January 1954 issue have been sent out to Technical Libraries to encourage subscription enquiries.

IRE Antennas and Waveguides Committee

Phil Smith became Chairman on May 1 of the IRE Antennas and Waveguides Committee for the next two-year term, succeeding Delmer Ports. The past two-year period has been an active and gratifying one for the Committee. During this time, the basic Definitions on Waveguide Terms were adopted by the Standards Committee and the Executive Committee, and were published at the end of last year. The Definitions on Waveguide Components have been completed and are now ready for consideration by the Standards Committee. A good start has been made on methods of measurement of waveguide and waveguide components.

Correspondence

We have received an interesting communication from W. Sichak of the Federal Telecommunication Laboratories at Nutley. His letter follows:

"For some reason or other I missed the first request to comment on Wheeler's proposal to split the PGAP into PGA and PGP.

"A specialist naturally prefers activities restricted to his own field. The basic questions are whether there is enough activity in any one field to justify its separation from a larger group and what it costs (in money, prestige, and effort) to maintain a separate group. Since there is no method of measuring "enough activity," a decision can be based only on opinions and personal judgments. A relative measure, however, can be obtained by comparing the proposed new group's probable activities with the activities of existing groups. If, for example, the split results in one group holding one meeting and publishing 50 pages annually while the average for all groups is 4 meetings and 250 pages, formation of a new group is probably not justified. At the moment the PGAP is seventh (in population) out of 21 groups. A split into two groups would reduce the groups to 15th and 16th (600 each), assuming equal numbers of antenna and propagation people. I don't know what would happen to the number of meetings and pages published annually, but a member of the administrative commit-

tee should be able to extrapolate these activities and determine the relative standing based on the past history of the groups. The cost (in money, but probably not in prestige or effort) can also be estimated in the same way. Such a study is worth presenting in the "news and views" section of the TRANSACTIONS if it is not too much work. After such a study is presented it may be worthwhile to poll the membership on forming two groups, keeping one group, or even joining with another group (such as the Microwave Theory and Techniques). Uninformed voting may lead to undesired results.

"The question raised by the IRE Committee on Antenna and Waveguide Definitions is a good one. IRE Standards are probably not used so much as they should be. One possible way to broaden their use is to have all published papers use the correct terms (whenever possible) as defined by the IRE Standards. This could be done by adding such a statement to the "Notice to Authors" section of each publication and by asking the reviewers to pay some attention to the use of standard terms. Enforcing this rule would be difficult for some broad papers, but should be relatively easy for such a specialized field as antennas."

PERSONAL

Dr. E. C. Jordan of the University of Illinois, who is well known for his work in the Antenna Field, has just been made Head of the Department of Electrical Engineering at the University of Illinois.

Professor V. H. Rumsey, who has been in charge of the Antenna Laboratory of the Ohio State University of Columbus, Ohio, has resigned and is joining the staff of the University of Illinois, taking charge of the research program which was supervised by Dr. Jordan. Professor Rumsey has been nominated as a member of the Administrative Committee of PGAP.

contributions

Virtual Source Luneberg Lenses*

G. D. M. PEELER†, MEMBER, IRE, K. S. KELLEHER‡, SENIOR MEMBER, IRE, AND H. P. COLEMAN†

Summary—**The portion of a spherical Luneberg lens contained between two plane reflectors has been investigated as a lens of reduced size and weight. If the reflectors pass through the center of the sphere, the resulting system produces several perfectly focused radiation beams, each appearing to originate from a virtual source on the surface of the full sphere. The virtual source positions and the position, beamwidth, and gain of the beams are accurately predicted from the spherical wedge angle and the source position. When the wedge angle is π/p, where p is an integer, rays with p reflections form the beam having the greatest gain at a displacement from the wedge bisector equal to the source displacement. For applications in which only this principal beam is desired, the gain of the unwanted beams can be reduced by absorption, reflection, or illumination taper.**

Scanning is achieved by moving the feed along the surface of the spherical wedge; if p is an odd integer, scanning can be obtained by moving the wedge past a fixed feed.

Experimental data were taken on a two-dimensional *X*-band model having a value of $p=1$. Good agreement was found with the predicted performance regarding beam position, beamwidth, and gain. The single, undesired beam was minimized by the use of absorbing material.

Introduction

WITHIN RECENT YEARS workers in microwave optics have given the Luneberg lens[1] much attention as a wide-angle scanning antenna because of its complete symmetry. No consideration, however, has been given to the utilization of only a portion of this lens, together with proper reflecting surfaces, as a means of reducing its size and weight. This combination of the lens section and the reflectors will be called a virtual source Luneberg lens. In this paper, some of the general properties of these Luneberg lenses are considered, and experimental data are presented for a lens of this type.

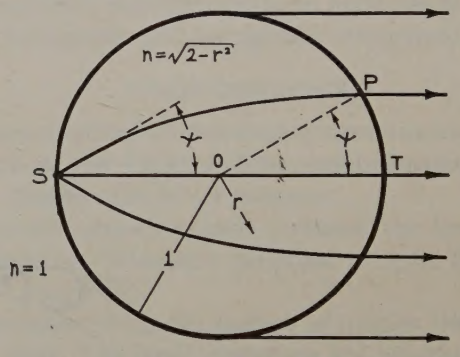

Fig. 1—Rays in a Luneberg lens.

The Luneberg lens is a spherical, variable-index-of-refraction system in which, for a unit-radius lens, the index of refraction n varies with the distance from the center r as $n=\sqrt{2-r^2}$. In this discussion, it is both convenient and sufficient to consider rays in a plane through the source and the lens center and if necessary, to extend these considerations to the full lens. As shown in Fig. 1, rays which leave the source S on the surface of the lens are focused into parallel rays. A ray leaving the source at an angle ψ from the diameter ST is radiated from the lens at the point P so that the radius OP forms an angle ψ with ST. The ray which leaves the source at $\psi=0$ propagates in a straight line through the center, while a ray leaving at $\psi=\pm\pi/2$ propagates along one fourth of the lens circumference before being radiated.

* Original manuscript received by PGAP, November 2, 1953.
† Naval Research Laboratory, Washington, D. C.
‡ Malpar, Inc., Alexandria, Va., formerly with the Naval Research Laboratory, Washington, D. C.
[1] R. K. Luneberg, "Mathematical Theory of Optics," Brown University Graduate School, Providence, R. I., 1944.

Virtual Source Lenses

Because of the symmetry in the Luneberg lens, plane reflecting surfaces may be placed through its center and the ray paths may be traced by the use of images. Consider a source at S (Fig. 2) displaced from the reference axis RO by an angle β (positive angles are measured counterclockwise). The addition of a single reflector perpendicular to RO will produce a virtual source. A typical ray, leaving S at an angle ψ, propagates through the lens and is reflected at this surface so that the angle of reflection equals the angle of incidence. This ray continues to propagate as if it originated at the virtual source S_1, which is the mirror image of S in the reflector (S_1 is displaced from RO through an angle $\pi-\beta$).

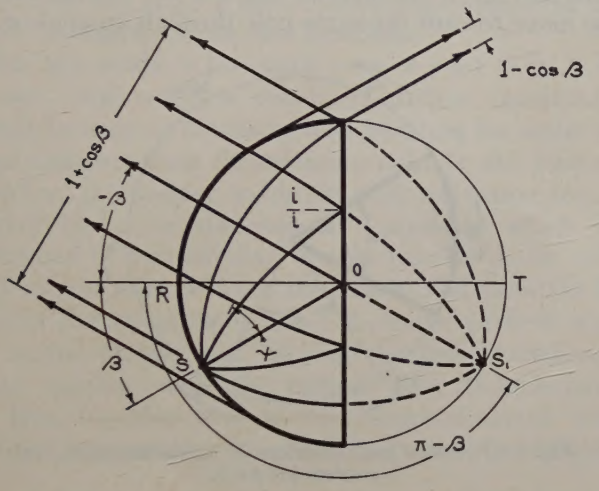

Fig. 2—Rays in a one-reflector virtual source Luneberg lens.

Therefore, all reflected rays are focused into a beam of parallel rays which is displaced at an angle $-\beta$ from RO as if the real source, in a full lens, were at S_1. If $\beta \neq 0$, some of the rays will be radiated without reaching the reflector and a focused beam of these "direct" rays is formed in the direction of SO.

This example is a special case of a spherical wedge in which the wedge angle is π. A general spherical wedge of angle α (Fig. 3) can also be examined by employing virtual sources. In this figure, the reference axis RO bisects the wedge angle and the source S is displaced from RO by an angle β. If $\alpha > \pi/2$ and $|\beta| + \alpha/2 > \pi/2$, a direct beam is formed; if $\alpha < \pi/2$, all rays are reflected and there is no direct beam. Figs. 3a and 3b show an arrangement with $\alpha > \pi/2$ and $|\beta| + \alpha/2 < \pi/2$. Let γ_1 be a boundary angle between two groups of rays leaving the source. In Fig. 3a, rays at angles γ from SO, such that $-\pi/2 \leqq \psi < \psi_1$, are reflected from the lower reflector and are radiated from the lens as if they originated at the virtual source S_1. As shown in Fig. 3b, rays leaving S at angles ψ, such that $\gamma_1 < \psi < 0$ also reflect from the lower reflector, propagate as if they originated at the virtual source S_1, reflect from the upper reflector, and are radiated from the lens at an angle $\pi-(2\alpha-\beta)$. Apparently, the radiated beam has been produced by the virtual source S_4 at an angle $-(2\alpha-\beta)$. By similar reasoning it can be shown that rays leaving S for positive values of ψ produce a virtual source S_2 at an angle $-(\alpha+\beta)$ and the corresponding radiation beam at an angle $\pi-(\alpha+\beta)$.

For any wedge angle α, similar techniques may be used to show that all the rays are radiated into perfectly focused beams as if they originated from their respective virtual sources. Table I, page 96, contains summary of virtual source and beam positions in terms of α and β. Notation for the virtual sources is given so that the order of their positions from S on a circumference of the full sphere is S_1, S_3, S_5, $\cdots$, in the positive direction and S_2, S_4, S_6, $\cdots$, in the negative direction. If α is small, the beams that might be formed by rays with few reflections are not radiated; the corresponding virtual source positions, however, are useful in determining the ray paths. For a given α, there is a maximum number of reflections so that a finite number of radiated beams exists.

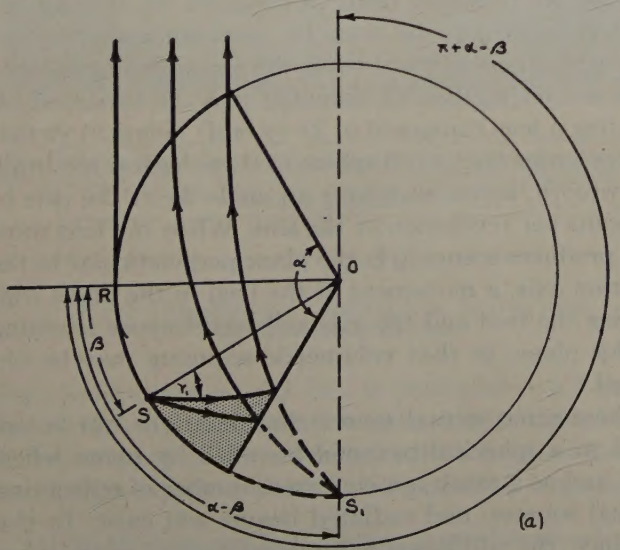

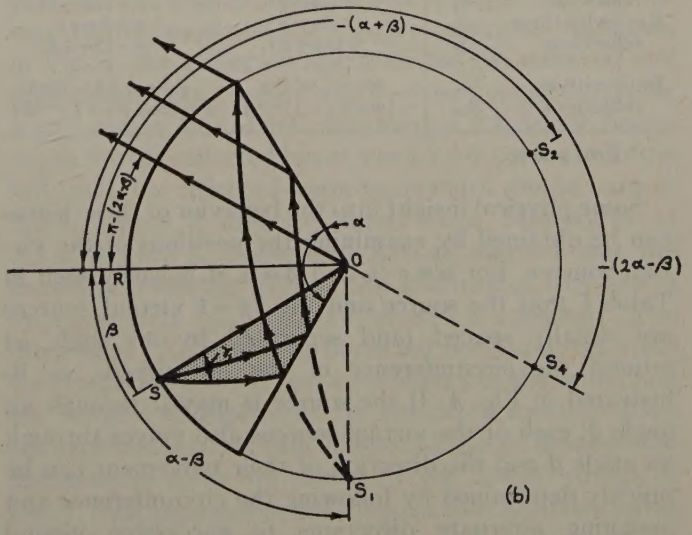

Fig. 3—Rays in a two-reflector virtual source Luneberg lens.

An idea of the relative gains of these beams may be obtained by noting that the beams formed from rays leaving the feed at large angles from the central ray are radiated from relatively small apertures and produce relatively large beamwidths. Also, owing to the illumination taper of a normal feed, these beams contain relatively little energy. The combination of these effects considerably reduces the gain of such beams, and as a result, the beams formed from rays leaving the feed at small angles from the central ray are the most important ones. Henceforth, the beam with the greatest gain will be referred to as the principal beam.

The most useful and interesting of these lenses are those which produce the principal beam at either $\pm\beta$ i.e., with the principal beam displacement from RO equal to the source displacement. This condition is achieved if $\alpha=\pi/p$, where p is an integer equal to the maximum number of reflections for any ray. Proof of this statement may be seen by examining the position of the beams formed from rays with p reflections. When $\alpha=\pi/p$, the virtual sources S_{2p-1} and S_{2p} coincide at the position $\pi+(-1)^p\beta$ to yield the principal beam at $-\beta$ for p odd and $+\beta$ for p even, so that there are $2p-1$ virtual sources. In order to calculate the minimum number of reflections for any ray, one notes that the circumferential ray must traverse a 90-degree arc before being radiated; this number is $p/2$ for p even and $(p-1)/2$ for p odd (except for $(p+1)/2$ when $\beta=0$). There are $p+1$ radiation beams, except when p is odd and $\beta=0$; in this event, there are p beams.

TABLE I
VIRTUAL SOURCE AND BEAM POSITIONS

Beam Formation	Virtual Source	Virtual Source Position	Radiated-Beam Position
Direct	S^*	β	$\pi+\beta$
Rays with one reflection	S_1	$\alpha-\beta$	$\pi+\alpha-\beta$
	S_2	$-(\alpha+\beta)$	$\pi-(\alpha+\beta)$
Rays with two reflections	S_3	$2\alpha+\beta)$	$\pi+2\alpha+\beta$
	S_4	$-(2\alpha-\beta)$	$\pi-(2\alpha-\beta)$
Rays with three reflections	S_5	$3\alpha-\beta$	$\pi+3\alpha-\beta$
	S_6	$-(3\alpha+\beta)$	$\pi-(3\alpha+\beta)$
...	...	...	...
Rays with m reflections	S_{2m-1}	$m\alpha+(-1)^m\beta$	$\pi+m\alpha+(-1)^m\beta$
	S_{2m}	$-\{m\alpha+(-1)^{m-1}\beta\}$	$\pi-\{m\alpha+(-1)^{m-1}\beta\}$

* Real source.

Some physical insight into the behavior of these lenses can be obtained by examining the positions of the virtual sources. For $\alpha=\pi/p$ and $\beta=0$, it is easily seen in Table I that the source and the $2p-1$ virtual sources are equally spaced (and separated by an angle α) around the circumference of the full sphere, as illustrated in Fig. 4. If the source is moved through an angle β, each of the virtual sources also moves through an angle β and the direction of their movement can be quickly determined by following the circumference and assigning alternate directions to successive virtual sources (as indicated by the arrows in Fig. 4). Since the virtual sources and the beams move through an angle equal to the source movement, the beam-factor for all beams is unity. For the case of p odd $(=3)$, the source and the principal virtual source $S_{5,6}$ move in opposite directions so that the principal beam position is $-\beta$. For a case of p even, say $p=4$, two virtual sources are added, one to each side of the full sphere, so that the source and the principal virtual source $S_{7,8}$ move in the same direction and the principal beam position is $+\beta$. It can be seen that the virtual sources and their beams move toward each other in pairs, and when $\beta=\alpha/2$, each of the pairs is combined into one virtual source. For these spherical wedge-shaped lenses, it can also be seen that if the source is moved toward one of the poles of the sphere (i.e., moved in a plane perpendicular to the plane in Fig. 4) through an angle ϕ the virtual sources also move toward the same pole through an angle ϕ.

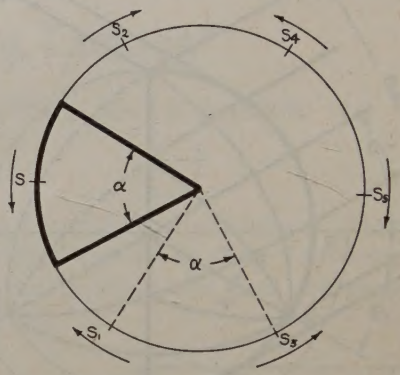

Fig. 4—Positions and directions of movement of virtual sources for $p=3$.

Two methods of utilizing these lenses for scanning antennas are apparent. One method consists of rotating the feed around the circumference of a stationary lens to obtain a scan of the principal beam over an angle α (or slightly less than α if the gain of the unwanted beams considered as a limiting factor). Another method, if p is odd, consists of rotating the lens past a stationary feed to obtain a scan over an angle 2α. If p is even, no scanning of the principal beam is obtained by this second method; this may be seen by inspecting the virtual source positions as was done in the preceding paragraph. This second method of scanning may be extended by rotating a lens composed of $2p$ (p odd) identical virtual source lenses (i.e., a full sphere of these lenses) to obtain a sawtooth, sector scan over an angle 2α at the rate of $2p$ scans per revolution of the lens. When the lens rotation produces scanning in the plane perpendicular to the rotation axis, a movement of the feed in the plane containing the feed and the axis will superimpose scanning in this plane, so that volumetric scanning may be obtained.

These same virtual source considerations can be applied to a spherical pyramid bounded by plane reflectors, and as a result, an increased number of reflections, virtual sources, and radiated beams will exist. In this instance, the additional parameters present in the num-

ber of reflecting planes and the angles between these planes provide such a large variety of possibilities that the development of a general system for determining positions of virtual sources and radiated beams does not seem advisable at this time.

Experimental Program

An experimental study was undertaken to determine the validity of virtual source considerations applied to the Luneberg lens and to measure the relative gain, position, beamwidth, and sidelobe level of the radiated beams. The virtual source considerations appeared quite valid, but there were some questions about the interaction of the radiated beams and the possible diffraction effects from nonsymmetrically illuminated apertures and from a high illumination appearing at a reflector edge for some feed positions.

For this study, a lens with $\alpha=\pi$ or $p=1$ (Fig. 2) was chosen. Ordinarily, a two-layer pillbox construction would be used to eliminate feed blocking for small feed displacements from the reference axis. In this instance, however, it was easy to obtain a virtual source lens by converting a two-dimensional Luneberg[2] which was composed of two circular, almost parallel plates and a polystyrene filler between the plates. The variation in n is obtained by utilizing the TE_{10} mode (E-field parallel to the plates) and varying the lens thickness, or plate spacing, with the radius. This 36-inch-diameter lens, together with a cross-sectional sketch which greatly exaggerates the plate curvature, is shown in

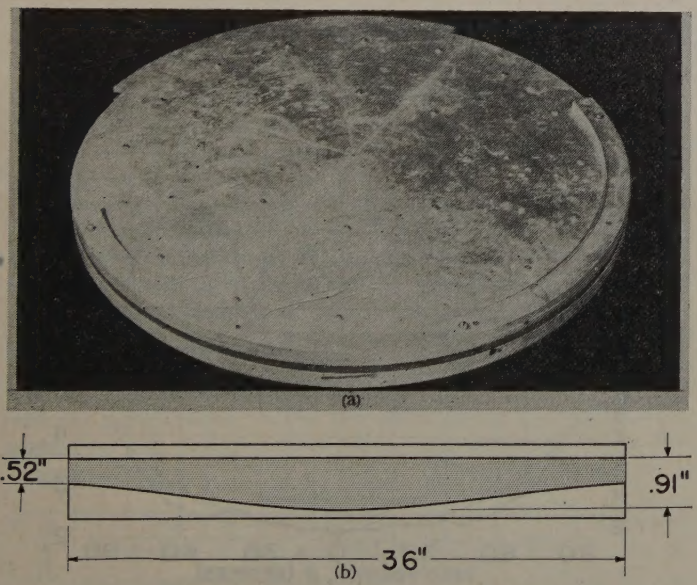

Fig. 5—Experimental Luneberg lens. (a) Top view. (b) Cross-sectional view.

Fig. 5. Designed at 3.2 cm, it produced a 2.2 degree beamwidth E-plane radiation pattern with sidelobes 18 db below peak power when fed with a source whose illumination tapers to 18 db below peak at $\psi=\pm\pi/2$. By placing a reflecting surface along a diameter of this lens a virtual source lens was obtained. The reflector was made $\frac{3}{16}$ inch in thickness to prevent energy from propagating past it. It was found experimentally that the original feed (the lower waveguide in Fig. 6) when used with this virtual source lens gave too much aperture blocking for small values of β. However, when the 90-degree curved section of waveguide (Fig. 6) was added so that only a small length of feed was left in the plane of the lens, aperture blocking was reduced considerably.

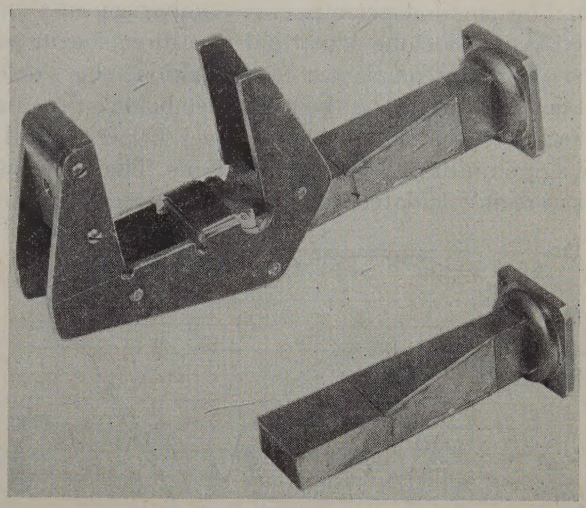

Fig. 6—Feeds for lens.

For a lens with $\alpha=\pi$, there is a virtual source at an angle $\pi-\beta$ and two radiation beams, a reflected beam at $-\beta$, and a direct beam at $\pi+\beta$. The reflected beam, formed of rays with one reflection, is the principal one. Although detailed radiation-pattern calculation for these beams is impractical and somewhat unneeded, an idea of the relative gains and beamwidths may be obtained by considering the energy in the beams and the projected effective apertures from which these beams are radiated. It will be assumed that the beamwidths are inversely proportional to the relative apertures and that relative gain is proportional to both the total energy in the beam and the relative apertures. As shown in Fig. 2, the projected apertures for the reflected and direct beams are $1+\cos\beta$ and $1-\cos\beta$, respectively, for a unit-radius lens. Then, assuming a 2.2 degree beamwidth for the reflected beam when $\beta=0$ (as found in the full lens), the reflected-beam beamwidth should vary as $2(2.2)/1+\cos\beta$ and the direct-beam beamwidth as $2(2.2)/1-\cos\beta$. Peeler and Archer[2] showed that the normalized electric field at the aperture of this lens is approximately $|E_a|=c\cos\psi$, where c is a constant. The integral of $|E_a|^2$ over the projected portion of the aperture radiating a beam yields the energy in the beam, and the integral multiplied by the projected aperture gives the expected relative gain. These calculated beamwidths and relative gains are shown by the dashed curves in Fig. 7. As β approaches ± 90 degrees the calculated gains of the two beams become equal and are 6 db below the reflected beam gain for $\beta=0$ since the power becomes

[2] G. D. M. Peeler and D. H. Archer, "A two-dimensional microwave Luneberg lens," Transactions, PGAP, p. 12; July, 1953.

equally divided between the two beams and each aperture approaches one half of the reflected beam aperture for $\beta=0$. As β approaches ± 90 degrees, both beamwidths approach 4.4 degrees or twice the reflected-beam beamwidth for $\beta=0$.

For comparison, Fig. 7 also contains experimental data obtained from E-plane radiation patterns taken at a frequency of 9,315 mc. In plotting these data, the peak power and sidelobe level for each pattern have been normalized to the reflected-beam peak power at $\beta=0$. This method permits easy comparison of the reflected-beam sidelobe level and the direct-beam peak power. For any particular feed position, the sidelobe level is found by taking the difference between the peak power and the indicated sidelobe level. Experimental results agree quite well with calculations. The beam positions were as calculated but were not plotted. The actual

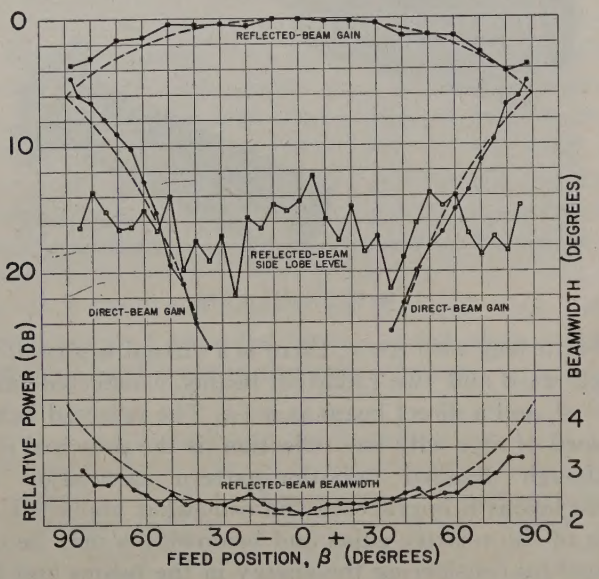

Fig. 7—Experimental and calculated data for a one-reflector virtual source lens.

beamwidth of the reflected beam is slightly greater than the calculated width for $|\beta|<40$ degrees and somewhat smaller for $|\beta|>50$ degrees. A sidelobe level of 14 db for the reflected beam is somewhat higher than might at first be expected; for $|\beta|<45$ degrees, however, an increase in the normal sidelobe level might be expected as a result of feed blocking. For the larger β's, the sidelobe level is probably due to the nonsymmetrical amplitude distribution over the reflected beam aperture. The direct-beam gain is below the sidelobe level of the reflected-beam for $|\beta|<55$ degrees, and the reflected-beam gain drops only 1.4 db at the edges of this range.

It can be noticed that data taken for this lens show asymmetry which can probably be attributed to some of the slight imperfections in the model. As a result of handling, the polystyrene around several of the bolt holes has fractured somewhat so that local refraction could occur in these regions. The fit between the reflector and the polystyrene appears good but a slight separation might also give local effects. There is no apparent asymmetry, hence a better model might provide symmetry and a lower sidelobe level.

For larger values of β, the direct-beam gain is greater than the sidelobe level of the reflected beam and could restrict the limit of operation for some applications. The direct-beam gain can be considerably reduced by placing absorbent material at the edges of the lens so that rays in the direct beam are absorbed without disturbing the

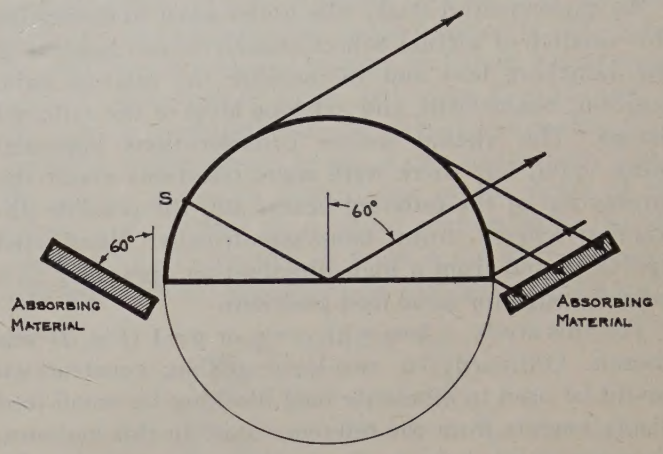

Fig. 8—One-reflector virtual source lens with absorbing material.

rays in the reflected beam. Fig. 8 shows one method of placing this material to absorb all the rays in the direct beam for $\beta=\pm 60$ degrees. For larger values of β, not all of the direct-beam rays will be absorbed, but only those rays with little energy will be radiated past the absorbers. Also, for $|\beta|>60$ degrees, the gain of the reflected beam should be reduced slightly as a result of the absorption of some of its energy.

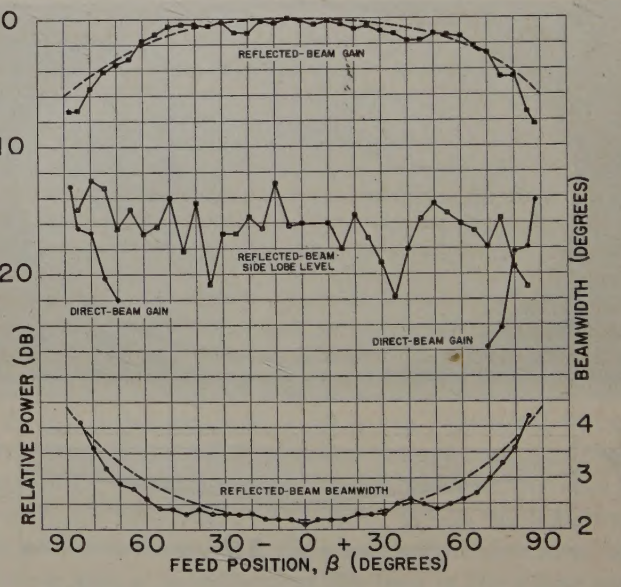

Fig. 9—Experimental data for a one-reflector virtual source lens with absorbing material.

Fig. 9 contains experimental data for this lens; microwave absorbing material[3,4] has been added as shown in Fig. 8. The direct-beam gain was reduced below the sidelobe level of the reflected beam for $|\beta|<80$ degrees. No effect on the reflected beam is noticed for $|\beta|<60$

[3] Manufactured by the Sponge Rubber Products Co.
[4] A. J. Simmons and W. H. Emerson, "Anechoic chamber for microwaves," *Tele-Tech & Elec. Ind.*, p. 47; July, 1953.

degrees; both gain and beamwidth, however, deteriorated slightly for $|\beta| > 60$ degrees. The calculated gain and beamwidth of the reflected beam for the lens without absorbing material is included for reference.

Another method for reducing the direct-beam gain appears feasible, although it was not checked experimentally. The 3/16 inch reflector can be extended beyond the edge of the lens so that part of the direct-beam energy is directed into the reflected beam. Since this energy is in phase with the energy already present in the reflected beam, this method should maintain the reflected-beam gain and beamwidth more constant with β.

The gain of unwanted beams can be further reduced by employing a greater illumination taper so that these beams contain less energy. This method has chief advantage for small values of β; as β approaches $\alpha/2$, its use entails less gain reduction. For the larger β's, however, tipping the feed so that the central ray is not directed at the wedge vertex would result in less energy in these beams. The use of more directive feeds is probably mandatory for small wedge-angle lenses which can produce several beams with gains comparable with the gain of the principal beam.

Conclusion

The analysis of virtual source Luneberg lenses shows that they can produce several perfectly focused radiation beams, each appearing to originate from a separate virtual source. The virtual source and beam positions can be accurately predicted from the spherical wedge angle α and the feed position β. In general, only a few of the beams are important; others contain little energy and have large beamwidth patterns so that their gain is below the diffraction sidelobe level of the important beams. For lenses with $\alpha = \pi/p$, where p is an integer, the beam with greatest gain has a position of $\pm\beta$, or has a displacement from the wedge bisector equal to that of the feed, so that this lens has a unity beam-factor.

Experimental data on a two-dimensional lens with $p = 1$ show good agreement with calculated beam positions, gain, and beamwidth. The sidelobe level from a spherical-wedge model or from a double-layer model would probably be somewhat lower than that found with this two-dimensional lens. Several methods for reducing the gain of unwanted beams were presented, and one method involving the addition of absorbing material was verified experimentally.

If a scan angle less than 120 degrees is desired, these lenses are useful for applications in which the size or weight of a full Luneberg sphere is prohibitive. For applications requiring several beams, where information from the beams need not be separated, one of these lenses can probably be designed to provide beams with the required gains in the desired directions.

A Theoretical and Experimental Study of the Recombination Coefficient in the Lower Ionosphere*

A. P. Mitra† and R. E. Jones‡

Summary—**The problem of recombination of electrons and ions in the lower ionosphere is studied both experimentally and theoretically. The experimental study involves analysis of new experimental data such as 150-kc radio wave absorption, polarization, and phase heights; absorption of short-wave galactic radiation; and E-region critical frequency, as well as recombination values already published. Then, by use of the theories of dissociative recombination and negative ions, a theoretical model is derived which is consistent with the experimental results. The values of the coefficient during night-time and during sudden ionospheric disturbances are discussed.**

THIS paper presents a tentative model of the height variation of the recombination coefficient, α, in the lower ionosphere, derived from published recombination values and a number of new experimental data such as 150-kc radio wave absorption, polarization, and phase heights; ionospheric absorption of short-wave galactic radiation and E-region critical frequency. Two methods have been used in estimating α. One is the well-known method of Appleton[1] and the other is from the time delay of the maximum of electron density from local noon. The latter involves the solution of the equation:

$$\frac{dN}{dt} = q - \alpha N^2$$

where N is the electron density and q is the rate of electron production. Approximate solution of the differential equation by means of successive approximation[2] yields the relation:

$$\tau(z) = \frac{1}{2\alpha(z) N_n(z)} \qquad (1)$$

where τ is the time of delay in seconds and N_n is the value of electron density at noon; all for a given height z. Eq. (1) has been derived for forms of the function $q(t)$ which may be represented by an even power

* Received by the PGAP, October 14, 1953. The research reported here has been sponsored by the Geophysics Research Division of the Air Force Cambridge Research Center, Air Research and Development Command, under Contract AF19(122)-44.

† Ionosphere Research Lab., The Pennsylvania State University. On leave from the Council of Scientific and Industrial Research, Government of India, and the Institute of Radiophysics and Electronics, University of Calcutta.

‡ Ionosphere Research Lab., The Pennsylvania State University.

[1] E. V. Appleton, "Regularities and irregularities in the ionosphere," *Proc. Roy. Soc.*, vol. A 162, p. 451; 1937.

[2] A. P. Mitra and R. E. Jones, Scientific Rep. No. 44, Ionosphere Research Lab., The Pennsylvania State University; March 25, 1953.

TABLE I

NEW EXPERIMENTAL VALUES OF α UNDER NORMAL CONDITIONS

Point on Fig. 1	Source	Experiment	Appropriate Electron Density Used (per cm^3)	Height (km)	α (cm^3 sec^{-1})
A	CRPL-F (Wash)	f_0E vs t	—	110	2.1×10^{-8}
B	Jones	150-kc h vs t	3,000	90	1.7×10^{-7}
C	Benner	150-kc absorption	600–800	80	$2\ \times10^{-7}$
D	Nearhoof	150-kc polarization	600–800	80	1.7×10^{-7}
E	Mitra and Shain	18.3-mc galactic absorption	600–800	80	$7\ \times10^{-7}$
F	Bracewell and Bain	16-kc h vs t	250	70	1.3×10^{-6}

series of constant and second degree terms. This includes variations of the type of Nicolet and Bossy[3] or the simple one of Chapman.

Although (1) refers primarily to a diurnal variation of *electron density*, it may also be employed for radio data on absorption, polarization, and phase height by suitable substitution. The absorption data utilized are the 150-kc results obtained at the Pennsylvania State University,[4] the medium short-wave absorption results obtained by Piggot,[5] and the 18.3-mc absorption results of Mitra and Shain[6] (in which the radio frequency radiations from the galaxy have been used and the contributions by the F_2-layer eliminated). For all these cases D-region absorption is nearly proportional to N_{max}, the electron density at the height of the maximum.[7,8] The polarization results used are the diurnal variations of the tilt angle ψ at 150 kc as observed at The Pennsylvania State University.[8,9] It is also shown[8] that ψ is nearly proportional to N_{max}. The phase-height results used are those of Jones[10] at 150 kc and of Bracewell and Bain[11] at 16 kc. It can be shown[12] that, in both cases, the phase height h around noon varies approximately linearly with the layer critical frequency, f_0, and may be approximated by

$$h \cong h_0 - Kf_0.$$

The daytime values of recombination coefficient obtained from the new experimental data are given in Table I, above.

The heights assigned are 80 km for D-region absorption and polarization effects and 90 and 70 km for the phase heights at 150 kc and 16 kc, respectively. These values of α have been plotted in Fig. 1 as well as the various published values for the level of the E-region maximum ionization ($\simeq$110 km) obtained from the diurnal variations of the E-region critical frequency, f_0E, and from eclipse studies. In addition, a new value of 2.1×10^{-8} cm^3/s obtained by analyzing later CRPL-F reports of f_0E at Washington, D. C., has been included (Point A). A mean curve has been drawn through the average value, indicated by a cross, at each height.

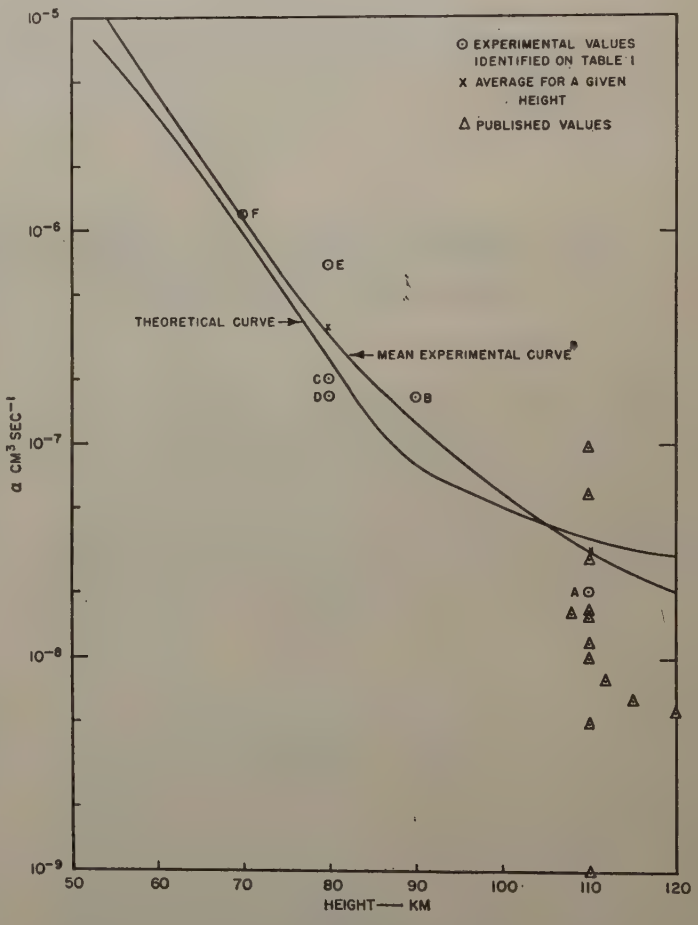

Fig. 1—Recombination coefficient as a function of height.

It should be noted here that a question may arise about attributing most of the short-wave absorption to D-region in the experiments of Mitra and Shain, and of

[3] M. Nicolet and L. Bossy, "Sur l'absorption des ondes courtes dans l'ionosphere," *Ann. Géophys.*, vol. 5, p. 275; 1949.
[4] A. H. Benner, Tech. Rep. No. 18, Ionosphere Research Laboratory, The Pennsylvania State University; January 30, 1952.
[5] As advised in a private communication.
[6] A. P. Mitra and C. A. Shain, "The measurement of ionospheric absorption using observations of 18.3 mc/s cosmic radio noise," *Jour. Atmos. Terr. Physics*, vol. 4, p. 204; 1953.
[7] J. C. Jaeger, "Equivalent path and absorption in an ionospheric region," *Proc. Phys. Soc.*, vol. 59, p. 87; 1947.
[8] J. M. Kelso, H. J. Nearhoof, R. J. Nertney, and A. H. Waynick, "The polarization of vertically incident long radio waves," *Ann. Géophys.*, vol. 7, p. 215; 1951.
[9] H. J. Nearhoof, Tech. Rep. No. 25, Ionosphere Research Lab., The Pennsylvania State University; August 20, 1951.
[10] R. E. Jones, Scientific Rep. No. 41, Ionosphere Research Lab., The Pennsylvania State University; August 15, 1952.
[11] R. N. Bracewell and W. C. Bain, "An explanation of radio propagation at 16 kc/s in terms of two layers below E-layer," *Jour. Atmos. Terr. Phys.*, vol. 2, p. 216; 1952.
[12] R. J. Nertney, Tech. Rep. No. 20, Ionosphere Research Lab., The Pennsylvania State University, March 15, 1951; "The lower E and D region of the ionosphere as deduced from long radio wave measurements," *Jour. Atmos. Terr. Phys.*, vol. 3, p. 92; 1953.

Piggot. In (1) it was shown that τ, the time delay of the maximum effect after local noon, is a function of height. To clarify the question, this function has been plotted in Fig. 2 from data to which satisfactory assignment of height is possible. These include the phase height asymmetry results at 16 and 150 kc, absorption and polarization asymmetries at 150 kc and f_0E asymmetry. Fig. 2, which *does not* include the short-wave absorption results, shows that, independently of the problem of the *amount* of absorption at the various levels, the time delay τ corresponding to the level of the maximum of the D-layer, about 80 km, is several times greater than that corresponding to the level of the E-region. Thus, even if considerable absorption takes place in E, the high values of τ found in the reference experiments must be due to the D-region.

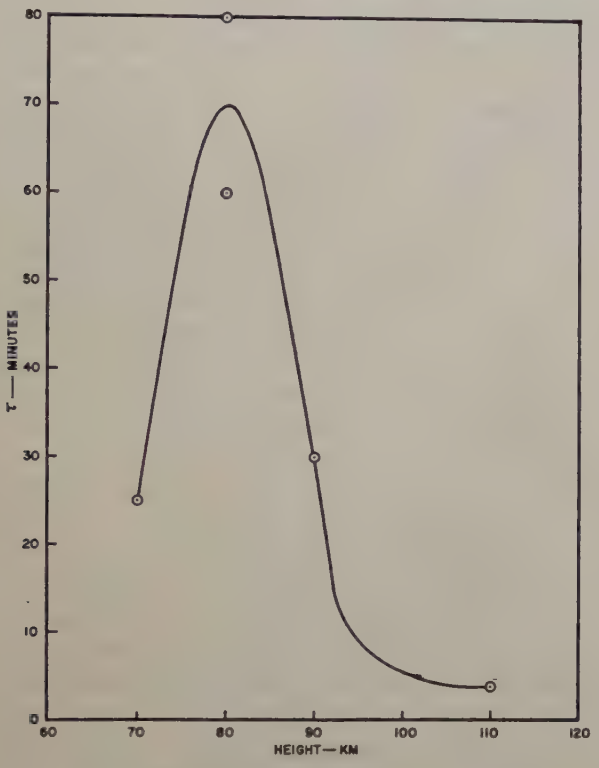

Fig. 2—Time delay (τ) as a function of height.

The recombination values so far discussed refer to daytime. Approximate estimates regarding the recombination coefficient at night have also been made from sunset data on 18.3-mc galactic absorption, 150-kc absorption and two days' diurnal variation of f_0E. While the f_0E results (where the existence of nonsolar sources of ionization complicate satisfactory interpretation of the data) show smaller values at night than during the day, the others, which refer to a level of 80 km, give larger values at night than during the day. The average ratio, for the latter, is about 4:1.

Estimates have also been made on the values of α during sudden ionospheric disturbances (SID), assumed to be due to solar flares. For this purpose a comparison was made of the variation of the width of the solar H_α line during a flare and the corresponding radio sudden phase anomaly (SPA) or sudden enhancement of atmospherics (SEA). These variations were plotted on the same time base with ordinate scales chosen so that their maxima occur at the same ordinate level. The data used here are from Ellison,[13] and Bracewell and Straker.[14] The analysis has been made in two different ways. In the first method the various curves have been compared at different levels and α calculated from[2]

$$\alpha = \frac{1 - \dfrac{\phi_2^2}{\phi_1^2}}{N_2 T}$$

where the subscripts 1 and 2 refer, respectively, to the reflection level at the time of the maximum of the effect and the reflection level at any subsequent time and the ϕ's are the phases corresponding to these reflection heights; T gives the difference between the times taken by SPA to recover to the level ϕ_2 and the line width to recover to its corresponding value.

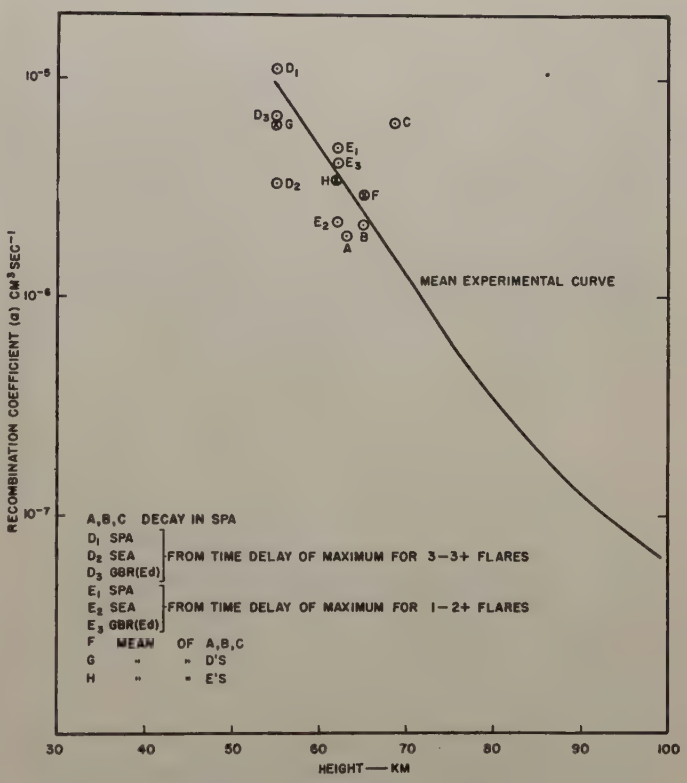

Fig. 3—Recombination coefficient as a function of height obtained from solar flare effects.

In the second method, measurements have been made of the time delays between the maximum of the ionospheric effect (SPA or SEA) and the maximum of the flare itself. Approximate heights of maximum effect have been assigned to these on the basis of an assumed 70 km for no effect. The results are plotted in Fig. 3

[13] M. A. Ellison, "Ionospheric effects of solar flares," *Royal Obs.*, Edinburgh, vol. 1, p. 53; 1950.

[14] R. N. Bracewell and T. W. Straker, "The study of solar flares by means of very long radio waves," *Mon. Not. R. Astr. Soc.*, vol. 109, p. 28; 1949.

along with the experimental mean curve of Fig. 1, which is for normal conditions. It may be seen that the flare values fall reasonably near the normal curve, having a spread which is no worse than the scatter of the normal points of Fig. 1. This implies that, for any height, the recombination coefficient remains constant during an SID and that the apparent change is fully explained by the decrease in height.

The theoretical interpretation of these results involves the theory of dissociative recombination and the theory of negative ion recombination. According to the former, recombination occurs by a process

$$XY^+ + e \rightarrow X' + Y'$$

while, according to the latter process, electrons attach to neutral particles to form negative ions which then disappear through a process of collisional detachment and ionic recombination. The negative ion theory has recently been examined by Bates and Massey[15] and has been found inadequate for Regions *E* and *F*. For these regions, dissociative recombination is supposed to predominate. For the lower ionosphere, however, the lack of sufficient experimental information has heretofore handicapped any adequate study of the possible recombination processes. In view of the experimental results reported in Table I and Fig. 1, it is now possible to examine these two theories for the lower ionosphere in some detail.

The effective recombination coefficient under the conditions where electrons disappear through negative ion formation *as well as* through dissociative recombination will be given by[15]

$$\alpha = [\alpha_D] + \left[\frac{\beta(O_2)n(O_2) + \beta(O)n(O)}{k(O)n(O) + \rho}\alpha_i\right] \quad (2)$$
$$= [\alpha_D] + [\lambda\alpha_i]$$

where

α_D is the coefficient of dissociative recombination
λ is the ratio of the concentration of negative ions to that of electrons
β is the coefficient of attachment
n is the particle density
k is the coefficient of collisional detachment
ρ is the coefficient of photodetachment
α_i is the coefficient of ionic recombination.

The first term is the contribution of dissociative recombination while the second term gives the negative ion contribution. Calculations with various possible values of the coefficients (β, k, ρ, and α_i) suggest that the latter can interpret observational results below about 80 km only, above which the discrepancy is serious. Although exact values of α_D are not available at present, the theoretical computations of Bates,[16] and Biondi and Brown's[17] microwave recombination values of O_2 (attributed to the dissociative process), extrapolated to low pressures, suggest that a value of about 3×10^{-8} cm³/s (required to explain the observational result at a height of 110 km) is quite likely for pressures of 10^{-4} mm of Hg or below, and a temperature of 300 degrees K. The theoretical curve of α from (2) obtained from such considerations is shown in Fig. 1. It seems likely, therefore, that recombination occurs mainly through negative ions between 70 and 80 km and through dissociation above 85 km. The region between 80 and 85 km is the transition region between the two processes.

At night when the photodetachment coefficient vanishes, the negative ion recombination coefficient is increased by a considerable amount; except perhaps in the height range 80–85 km. The dissociative recombination, however, is not appreciably affected at night, so that, in regions where the dissociative recombination is large, the increase in $\lambda\alpha_i$ (see (2)) at night may not affect the actual coefficient to a large extent. Calculations show that for the case in which dissociative recombination predominates above 85 km and negative ion recombination below 80 km, there is a theoretical increase of α from 2.4×10^{-7} cm³/s to 6.5×10^{-7} cm³/s at 90 km. The observed ratio of 4:1 of nighttime to daytime recombination coefficients at 80 km is, therefore, explained. However, it is necessary to obtain better estimates of night values of α before definite conclusions can be drawn.

Lastly, the experimental result that, for any height, the recombination coefficient remains constant during an SID indicates that λ is not changed at all and, hence, any enhancement of electron density must be interpreted by an enhancement in q. An adequate enhancement in q capable of producing the observed enhancement of ionization and the large changes in phase height as observed at 16 kc may be obtained on the single assumption that the normal as well as the SID ionizations are due to the photoionization of *NO* by L_α radiation.

[15] D. R. Bates and H. S. W. Massey, "The negative ion concentration in the lower ionosphere," *Jour. Atmos. Terr. Phys.*, vol. 2, p. 1; 1951.

[16] D. R. Bates, "Electron recombination in helium," *Phys. Rev.*, vol. 77, p. 718, vol. 79, p. 492; 1950.

[17] M. A. Biondi and S. C. Brown, "Measurements of ambipolar diffusion in helium," *Phys. Rev.*, vol. 75, p. 1700, vol. 76, p. 1697; 1949.

Low Frequency Waves on Transmission Lines of Composite Section*

R. W. KLOPFENSTEIN†, MEMBER, IRE

Summary—**Three types of transmission lines are analyzed, and it is found that the principal wave is not transverse electromagnetic in transmission lines for which the medium between the conducting boundaries is other than a homogeneous isotropic dielectric. Calculations of characteristic impedance and velocity of propagation on the basis of electrostatic and magnetostatic field distributions are accurate in the low-frequency limit. The cut-off frequency for the first higher order mode lies between those that would be obtained if the transmission lines were entirely filled with one dielectric material or the other.**

Introduction

MUCH OF THE work done to date on the propagation of electromagnetic waves along transmission lines and in wave guides has been concerned with the case in which an isotropic homogeneous medium was bounded by a conducting surface or conducting surfaces. A limited amount of work, however, has been done on wave guides of composite section.[1,2,3] This paper deals with the propagation of low-frequency waves on transmission lines of composite section. The use of such transmission lines is often desirable due to mechanical considerations. One approach to the analysis of such transmission lines would be through the consideration of electrostatic and magnetostatic field configurations as in the case of transmission lines of uniform cross-section. That such an approach is not strictly valid is one of the results of the work presented here.

Attention is focused on the propagation of the principal wave in three types of transmission lines of composite section. While two of these transmission line types have been previously considered[4] they are discussed here from a somewhat different point of view. Although a knowledge of the cut-off frequencies for higher order modes is not required in the analysis of principal wave propagation, it is essential in application to have a knowledge of the cut-off frequency of at least the first higher order mode since a transmission line is not ordinarily usable above this frequency. The cut-off frequencies for the higher order modes in the transmission lines analyzed have been obtained.

Conventional transmission line theory is exactly applicable when a transverse electromagnetic wave is propagated in a transmission line. In general, for a transmission line for which the medium between conductors is not isotropic and homogeneous the transverse electromagnetic wave cannot be propagated at even the lowest frequencies, but rather the principal wave is of a more complicated type which depends for its exact form on the configuration of the transmission line. One of the aims of this paper is to determine to what extent conventional transmission line theory is applicable to principal wave propagation in transmission lines of composite section. The results are presented in terms of an effective dielectric constant for the transmission line. This effective dielectric constant may be used in the calculation of the characteristic impedance and velocity of propagation for the transmission line. In the cases treated the effective dielectric constant is somewhat higher than that which would be predicted on the basis of an electrostatic capacity calculation.

Definition of Symbols

The symbolization to be used is essentially similar to that used by Stratton.[5] The mks system of rationalized units has been used throughout; the time dependence has been introduced through the factor $e^{-i\omega t}$. The Z axis has been taken as the direction of wave propagation in the co-ordinate systems employed. For convenience in reference, the symbols used are set forth below:

i satisfies the equation $i^2 = -1$.
t denotes the time variable expressed in seconds.
ω is the angular velocity in radians per second of a periodic function of time.
x, y, and z are the co-ordinates in a rectangular co-ordinate system.
$\hat{i}$, $\hat{j}$, and $\hat{k}$ are the unit vectors directed respectively along the X, Y, and Z axes.
r, θ, and z are the co-ordinates in a cylindrical co-ordinate system.
$\overline{\mathcal{E}}$ and $\overline{\mathcal{H}}$ are the electric and magnetic field vectors respectively.
$\overline{E}$ and $\overline{H}$ are the electric and magnetic field vectors respectively from which the time and z dependence have been removed.
$\overline{E}_c$ and $\overline{H}_c$ are respectively the parts of $\overline{E}$ and $\overline{H}$ lying in a plane perpendicular to the Z axis.
E_z and H_z are respectively the components of $\overline{E}$ and $\overline{H}$ along the Z axis.
μ denotes the magnetic permeability of a medium.
ϵ denotes the electric permittivity of a medium.
k is a quantity arising in the solution of Maxwell's

* Revised manuscript received by the PGAP, April 5, 1954.
† R.C.A. Laboratories Div., Princeton, N. J., formerly Mathematics Dept., Iowa State College, Ames, Ia.
[1] Office of Scientific Research and Development, National Defense Research Committee, "Principles of Microwave Circuits," McGraw-Hill Book Co., Inc., New York, N. Y., 1st ed.; 1948.
[2] L. Pincherle, "Electromagnetic waves in metal tubes filled longitudinally with two dielectrics," *Phys. Rev.*, 2nd ser., vol. 66, pp. 118–130; 1944.
[3] J. Van Bladel and T. J. Higgins, "Cut-off frequency in two dielectric layered rectangular waveguides," *Jour. Appl. Phys.*, vol. 22, pp. 329–334; 1951.
[4] N. Marcuvitz, "Waveguide Handbook," McGraw-Hill Book Co., Inc., New York, N. Y., pp. 388–393, 396–397; 1951.
[5] J. A. Stratton "Electromagnetic Theory," McGraw-Hill Book Co., Inc., New York, N. Y., 1st ed.; 1941.

equations which, for a nonconducting medium, is defined by the equation $k^2=\omega^2\mu\epsilon$.

h is a separation constant which arises in the solution of Maxwell's equations. It is inversely proportional to the phase velocity of the wave in the z direction.

ϵ^*, defined by the equation $h^2=\omega^2\mu\epsilon^*$, is an effective dielectric constant for composite transmission lines.

x_0, L, a, b, and c are used in denoting the dimensions of the transmission lines considered.

$J_n(z)$, $N_n(z)$, $I_n(z)$, and $K_n(z)$ denote Bessel functions of the first and second kind and modified Bessel functions of the first and second kind respectively.

Other symbols not defined here will be defined when they are used. Subscripts on the symbols above will be used to associate them with a given medium.

General Theory

For the purposes of this paper only waves propagated in a single direction will be considered, and the direction of propagation will be taken as the positive Z axis. The electric and magnetic field vectors may then be represented as follows:

$$\overline{\mathcal{E}} = \overline{E}e^{i(hz-\omega t)} = (\overline{E}_c + \hat{k}E_z)e^{i(hz-\omega t)}, \tag{1}$$

and

$$\overline{\mathcal{H}} = \overline{H}e^{i(hz-\omega t)} = (\overline{H}_c + \hat{k}H_z)e^{i(hz-\omega t)}, \tag{2}$$

where $\overline{E}$, $\overline{E}_c$, $\overline{H}$, and $\overline{H}_c$ are vectors, and E_z and H_z are scalars which depend only on the co-ordinates in a plane perpendicular to the Z axis. $\overline{E}_c$ and $\overline{H}_c$ lie entirely in a plane perpendicular to the z axis.

From Maxwell's equations it is found that E_z and H_z must satisfy the scalar wave equations

$$\nabla^2 E_z + (k^2 - h^2)E_z = 0, \tag{3}$$

and

$$\nabla^2 H_z + (k^2 - h^2)H_z = 0, \tag{4}$$

where

$$k^2 = \omega^2\mu\epsilon. \tag{5}$$

Furthermore, the other components of the field vectors are obtained from E_z and H_z according to the relations[3]

$$(k^2 - h^2)\overline{E}_c = ih\nabla E_z - i\omega\mu\hat{k} \times \nabla H_z, \tag{6}$$

and

$$(k^2 - h^2)\overline{H}_c = ih\nabla H_z + i\omega\epsilon\hat{k} \times \nabla E_z, \tag{7}$$

provided $k^2-h^2\neq 0$. If $k^2-h^2=0$, the wave propagated is of the transverse electromagnetic type.

Equations (6) and (7) show clearly that the very existence of a TEM type wave implies that $h=\pm k$. That is, if a TEM type wave exists, it must be propagated at the characteristic velocity associated with the medium in which it exists. The TEM wave may be propagated in the case of a homogeneous, isotropic, nonconducting medium bounded by perfectly conducting surfaces for which the wave guide cross-section is multiply connected;[6] and in this case the transmission characteristics of the system may be predicted exactly from conventional transmission line theory using capacitance and inductance per unit length calculated from static field distributions.

The transmission lines considered in this paper are not of the type just described, and their transmission characteristics can be predicted accurately only through a direct solution of Maxwell's equations. The usual boundary conditions apply at the conducting surfaces and at the dielectric interfaces.[5] That is, (a) at a perfectly conducting boundary, the tangential electric field as well as the normal derivative of the tangential magnetic field vanishes, and (b) at a dielectric interface the tangential components of electric and magnetic fields are continuous.

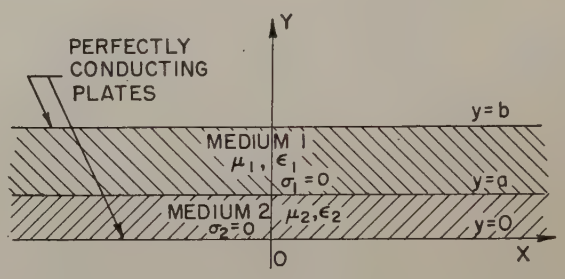

Fig. 1—Composite parallel plate transmission line of first type.

The Composite Parallel Plate Line

Although the parallel plate line as such is never met with in practice due to its infinite extent, the parallel plate line of finite extent is often used and results with regard to the infinite parallel plate line are useful in predicting its performance in situations where edge effects can be ignored. Furthermore, the performance of parallel plate structures is closely related to the performance of the corresponding coaxial line structures for which the spacing between conductors is small compared to their radii. Parallel plate structures furnish a particularly instructive example for analysis due to the relative simplicity of the mathematical expressions encountered.

Composite Line for which the Surface of Discontinuity Is Parallel to the Conducting Plates

The configuration considered here is shown in Fig. 1. The fields E_z and H_z, which satisfy (3) and (4) in rectangular co-ordinates with y variation only are

$$E_{z1} = A_1 \sin(\lambda_1 y + \delta_{11}), \tag{8}$$

$$H_{z1} = B_1 \sin(\lambda_1 y + \delta_{12}), \tag{9}$$

$$E_{z2} = A_2 \sin(\lambda_2 y + \delta_{21}), \tag{10}$$

[6] W. H. Watson, "The Physical Principles of Waveguide Transmission and Antenna Systems", Oxford University Press, London, p. 47; 1947.

and

$$H_{z2} = B_2 \sin(\lambda_2 y + \delta_{22}), \tag{11}$$

where

$$\lambda_1^2 = k_1^2 - h^2, \tag{12}$$

and

$$\lambda_2^2 = k_2^2 - h^2. \tag{13}$$

The additional field components are obtained from (6) and (7).

When the boundary conditions at the perfectly conducting boundaries and at the boundary between the dielectric materials are applied the following set of linear homogeneous equations in the four quantities A_1, A_2, B_1, and B_2, is obtained.

$$A_1 \sin \lambda_1(a-b) - A_2 \sin \lambda_2 a = 0, \tag{14}$$

$$A_1 \omega \epsilon_1 \lambda_2 \cos \lambda_1(a-b) - A_2 \omega \epsilon_2 \lambda_1 \cos \lambda_2 a = 0, \tag{15}$$

$$B_1 \cos \lambda_1(a-b) - B_2 \cos \lambda_2 a = 0, \tag{16}$$

and

$$B_1 \omega \mu_1 \lambda_2 \sin \lambda_1(a-b) - B_2 \omega \mu_2 \lambda_1 \sin \lambda_2 a = 0. \tag{17}$$

For the above set of four equations in four unknowns (A_1, A_2, B_1, B_2) to have a nonzero solution, it is necessary and sufficient that the determinant of the coefficient matrix be zero. In this case, the coefficient matrix has the form

$$F = \begin{vmatrix} a_{11} & a_{12} & 0 & 0 \\ a_{21} & a_{22} & 0 & 0 \\ 0 & 0 & a_{33} & a_{34} \\ 0 & 0 & a_{43} & a_{44} \end{vmatrix} = \begin{pmatrix} F_1 & 0 \\ 0 & F_2 \end{pmatrix}, \tag{18}$$

where

$$F_1 = \begin{pmatrix} a_{11} & a_{12} \\ a_{21} & a_{22} \end{pmatrix}, \tag{19}$$

and

$$F_2 = \begin{pmatrix} a_{33} & a_{34} \\ a_{43} & a_{44} \end{pmatrix}. \tag{20}$$

A Laplace expansion of the determinant of F yields

$$|F| = |F_1||F_2|. \tag{21}$$

Therefore, $|F| = 0$ if and only if $|F_1| = 0$ or $|F_2| = 0$. Physically, this means that the permissible wave types can be separated into two types; namely, transverse electric waves corresponding to solutions of (16) and (17), and transverse magnetic waves corresponding to solutions of (14) and (15).

Expansion of the determinants yields

$$\frac{\epsilon_1}{\epsilon_2}\sqrt{\frac{k_2^2 - h^2}{k_1^2 - h^2}} = -\frac{\tan\left[(b-a)\sqrt{k_1^2 - h^2}\right]}{\tan\left[a\sqrt{k_2^2 - h^2}\right]}, \tag{22}$$

for transverse magnetic waves, and

$$\frac{\mu_1}{\mu_2}\sqrt{\frac{k_2^2 - h^2}{k_1^2 - h^2}} = -\frac{\tan\left[a\sqrt{k_2^2 - h^2}\right]}{\tan\left[(b-a)\sqrt{k_1^2 - h^2}\right]} \tag{23}$$

for transverse electric waves. Values of h satisfying these equations represent permissible wave types in the transmission line.

Cut-off frequencies for higher order modes are obtained in the usual fashion by setting $h=0$ in (22) and (23). Both of these equations can then be written

$$\sqrt{\frac{\epsilon_2}{\epsilon_1}} = -\frac{\tan\left[k_1 a\sqrt{\frac{\epsilon_2}{\epsilon_1}}\right]}{\tan\left[k_1(b-a)\right]}. \tag{24}$$

where it is assumed that $\mu_2 = \mu_1$ as is the case with materials normally used in practice. It is further assumed that $\epsilon_2 > \epsilon_1$ for convenience in discussion. There exists a denumerable set of wave types whose cut-off frequencies correspond to the positive values of k_1 which are roots of (24). Moreover, the cut-off frequencies of the transverse magnetic modes and the transverse electric modes coincide.

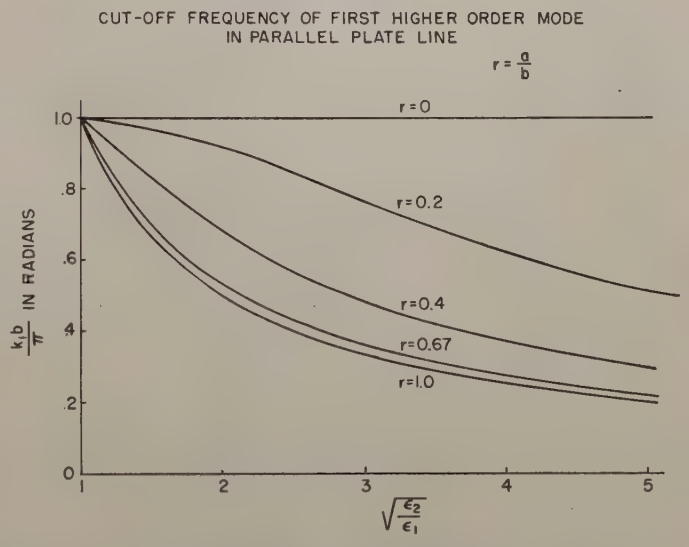

Fig. 2—Cut-off frequencies for composite parallel plate transmission lines. Refer to Fig. 1 for notation.

The first positive root of (24) is plotted in Fig. 2 for several typical cases. It is interesting to note the large effect of a given amount of dielectric material on the cut-off frequency of the first higher order mode. The cut-off frequency of the first higher order mode is lowered nearly as much by filling the line to two-thirds depth with a given dielectric material as it is by filling the line completely with the dielectric material.

It is of particular interest to examine the principal wave type in this configuration. Equation (22) has a positive real root for arbitrarily low frequencies while (23) does not ($\mu_1 = \mu_2$). Therefore, the principal wave is of the transverse magnetic type. Noting that the first positive real root of (22) satisfies

$$k_1 < h < k_2, \tag{25}$$

and setting

$$h^2 = \omega^2 \mu \epsilon^* \tag{26}$$

where ϵ^* is an effective dielectric constant, (22) may be written

$$\frac{\epsilon_1}{\epsilon_2}\sqrt{\frac{1-\frac{\epsilon^*}{\epsilon_2}}{\frac{\epsilon^*}{\epsilon_1}-1}} = \frac{\tanh\left[k_1(b-a)\sqrt{\frac{\epsilon^*}{\epsilon_1}-1}\right]}{\tan\left[k_2 a\sqrt{1-\frac{\epsilon^*}{\epsilon_2}}\right]}. \tag{27}$$

The value of ϵ^* which is the first positive root of (27) may be used for calculating the velocity of propagation and the characteristic impedance of the transmission line for the principal wave.

At very low frequencies, the tangent and hyperbolic tangent functions may be approximately represented by their arguments, and the first positive root of (27) is then given approximately by

$$\epsilon^* \simeq \frac{b\epsilon_1\epsilon_2}{a\epsilon_1 + (b-a)\epsilon_2}, \tag{28}$$

which is the value of ϵ^* that would be predicted on the basis of a calculation of the electrostatic capacity between the parallel plates. The exact value of ϵ^* computed from (27) will be somewhat larger than that indicated by (28).

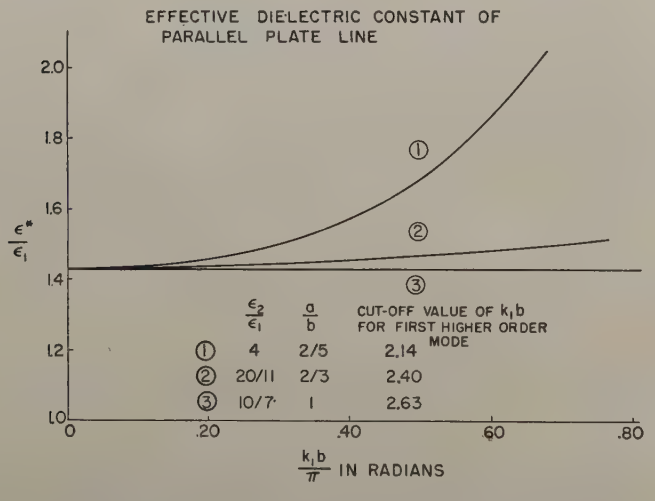

Fig. 3—Effective dielectric constant for composite parallel plate transmission line. Refer to Fig. 1 for notation.

Values of the effective dielectric constant are plotted against a factor which is proportional to frequency for several cases in Fig. 3. The three cases shown have the same electrostatic capacity per unit width between the plates. It is seen that the results vary widely for different proportioning of the two dielectrics, and that there is a significant difference between the value indicated by an electrostatic approximation and the actual value in many cases.

When the expressions for the field vectors are obtained for the principal wave, it is found that a longitudinal component of the electric field exists at all frequencies but that this component is ninety degrees out of phase with the transverse components of the electric and magnetic fields. Thus, no real power is transferred across the dielectric interface, but rather, an exchange of reactive power takes place. The magnitude of the field vector components is plotted for two typical cases in Fig. 4.

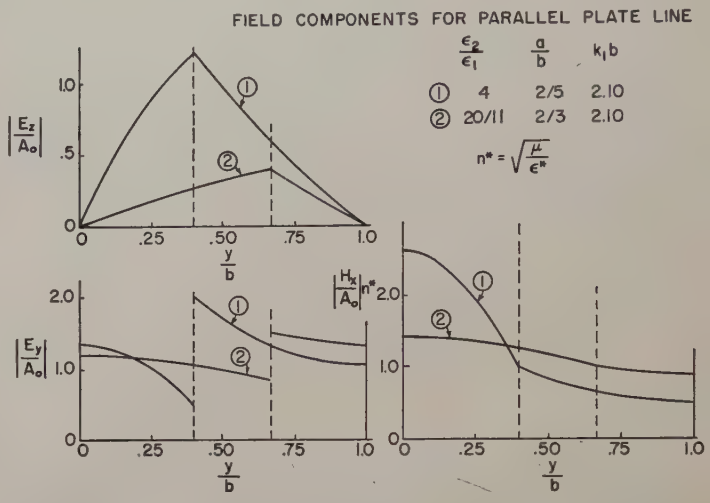

Fig. 4—Field components for composite parallel plate transmission lines. Refer to Fig. 1 for notation.

The results of this section may be summarized as follows. The transverse electromagnetic wave cannot be propagated in this case unless $k_1 = k_2$. The principal wave is of transverse magnetic type, and the effective dielectric constant for principal wave propagation depends upon frequency in general. At very low frequencies the effective dielectric constant is given approximately by an electrostatic capacity calculation. The cut-off frequency for the first higher order mode lies between those which would be obtained if the line were completely filled with dielectric of one type or the other.

Composite Line for which the Surfaces of Discontinuity are Perpendicular to the Conducting Plates

In the problem considered here the surfaces of discontinuity are perpendicular to the conducting parallel plates. A denumerable number of such surfaces of discontinuity are present in the parallel plate line, and the structure is periodic along the X axis with a period of $2L$. A cross section of the line is shown in Fig. 5. The fields, E_z and H_z, which satisfy (3) and (4) in rectangular co-ordinates are

$$E_{z1} = A_1 \sin(\lambda_{11}x + \delta_{11}) \sin(\nu_{11}y + \alpha_{11}), \tag{29}$$

$$H_{z1} = B_1 \sin(\lambda_{12}x + \delta_{12}) \cos(\nu_{12}y + \alpha_{12}), \tag{30}$$

$$E_{z2} = A_2 \sin(\lambda_{21}x + \delta_{21}) \sin(\nu_{21}y + \alpha_{21}), \tag{31}$$

and

$$H_{z2} = B_2 \sin(\lambda_{22}x + \delta_{22}) \cos(\nu_{22}y + \alpha_{22}), \tag{32}$$

where

$$\lambda_{ij}^2 + \nu_{ij}^2 = k_i^2 - h^2. \tag{33}$$

A consideration of the boundary conditions leads to the conclusion that

$$\nu_{11} = \nu_{12} = \nu_{21} = \nu_{22} = \frac{n\pi}{a}, \qquad \alpha_{ij} \equiv 0, \tag{34}$$

where n is restricted to positive integral values or zero, and that

$$\lambda_{21} = \lambda_{22}, \tag{35}$$

henceforth to be denoted by λ_2 and that

$$\lambda_{11} = \lambda_{12}, \tag{36}$$

henceforth to be denoted by λ_1. The requirement that the wave functions for two corresponding points in media of the same type shall be equal leads to a difference equation which determines a relation between the δ_{ij} for successive media of the same type. Ultimately by applying the boundary conditions at the dielectric

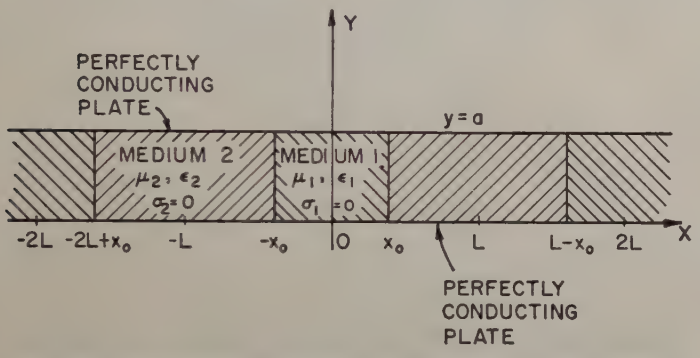

Fig. 5—Composite parallel plate transmission line of second type.

interfaces a set of eight homogeneous linear equations in eight unknowns is obtained similar to (14) through (17). Upon setting the determinant of the coefficient matrix equal to zero, it is found that the determinantal equation is factorable. A nonzero solution to the system of equations exists if and only if

$$\omega^2\mu_2\epsilon_1 \frac{\tan(\lambda_1 x_0)}{\tan[\lambda_2(L-x_0)]} + \omega^2\mu_1\epsilon_2 \frac{\tan[\lambda_2(L-x_0)]}{\tan(\lambda_1 x_0)} + \frac{(k_2^2-h^2)^2\lambda_1^2k_1^2 + (k_1^2-h^2)^2\lambda_2^2k_2^2 + h^2\frac{\pi^2n^2}{a^2}(k_2^2-k_1^2)^2}{\lambda_1\lambda_2(k_1^2-h^2)(k_2^2-h^2)} = 0, \tag{37}$$

or

$$\omega^2\mu_2\epsilon_1 \frac{\tan[\lambda_2(L-x_0)]}{\tan(\lambda_1 x_0)} + \omega^2\mu_1\epsilon_2 \frac{\tan(\lambda_1 x_0)}{\tan[\lambda_2(L-x_0)]} + \frac{(k_2^2-h^2)^2\lambda_1^2k_1^2 + (k_1^2-h^2)^2\lambda_2^2k_2^2 + h^2\frac{\pi^2n^2}{a^2}(k_2^2-k_1^2)^2}{\lambda_1\lambda_2(k_1^2-h^2)(k_2^2-h^2)} = 0; \qquad n \neq 0. \tag{38}$$

It is noted that (37) and (38) can be written as quadratic forms in $\tan(\lambda_1 x_0)$ and $\tan[\lambda_2(L-x_0)]$, and, hence, they are factorable into linear expressions in these quantities. Except for the case $n=0$, the wave types are neither transverse electric nor transverse magnetic but rather a combination of the two types. In the event $n=0$, (37) and (38) are replaced by

$$\frac{\mu_2}{\mu_1}\sqrt{\frac{k_1^2-h^2}{k_2^2-h^2}} = -\frac{\tan(x_0\sqrt{k_1^2-h^2})}{\tan[(L-x_0)\sqrt{k_2^2-h^2}]}, \tag{39}$$

and

$$\frac{\mu_1}{\mu_2}\sqrt{\frac{k_2^2-h^2}{k_1^2-h^2}} = -\frac{\tan(x_0\sqrt{k_1^2-h^2})}{\tan[(L-x_0)\sqrt{k_2^2-h^2}]}; \tag{40}$$

in which case the waves are of the transverse electric type. Equation (40) has a positive real root for arbitrarily low frequencies which corresponds to the principal wave. Upon rewriting this equation in terms of the effective dielectric constant defined by (26) it is found that

$$\frac{\mu_1}{\mu_2}\sqrt{\frac{\epsilon_2}{\epsilon_1}}\sqrt{\frac{1-\frac{\epsilon^*}{\epsilon_2}}{\frac{\epsilon^*}{\epsilon_1}-1}} = \frac{\tanh\left[k_1x_0\sqrt{\frac{\epsilon^*}{\epsilon_1}-1}\right]}{\tan\left[k_2(L-x_0)\sqrt{1-\frac{\epsilon^*}{\epsilon_2}}\right]}. \tag{41}$$

It is assumed that $\mu_1=\mu_2$ and that $\epsilon_2>\epsilon_1$ as before.

At very low frequencies the hyperbolic tangent and tangent functions may be represented approximately by their arguments. When done it is found from (41) that

$$\epsilon^* \simeq \frac{x_0\epsilon_1}{L} + \left(1-\frac{x_0}{L}\right)\epsilon_2, \tag{42}$$

which is the same value of ϵ^* that would be predicted on the basis of electrostatic capacity calculations. The exact values of ϵ^* obtained from (41) will be somewhat larger than those given by (42). Values of the effective dielectric constant for several typical cases are plotted against a factor proportional to frequency in Fig. 6.

It is noted that the principal wave here is of the transverse electric type while for the previous case it was of the transverse magnetic type. When expressions for the field vectors are obtained it is found that a longitudinal component of magnetic field exists at all frequencies and that this component of magnetic field is ninety degrees out of phase with the transverse components of the field vectors so that again no real power is transferred across the dielectric interfaces. The magnitude of the field components is plotted for two typical cases in Fig. 7.

The cut-off frequencies for higher order modes may be determined by setting $h=0$ in (37) and (38), or in the

special case $n=0$ by setting $h=0$ in (39) and (40).

The transmission line parameters and dimensions will determine which of these equations will yield the lowest cut-off frequency. However, if $a<L$ the first positive root will be determined from (39). In this case, the curves of Fig. 2 may be used to predict the cut-off frequency of the first higher order mode by replacing k_1b by k_1L and letting $r=1-(x_0/L)$.

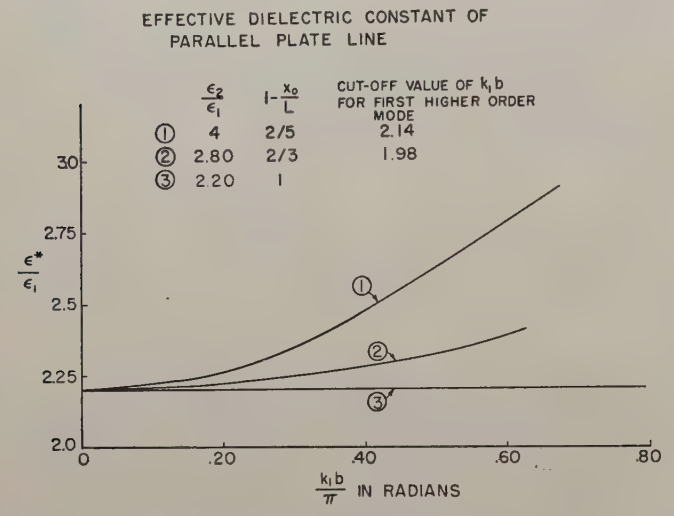

Fig. 6—Effective dielectric constant for composite parallel plate transmission lines. Refer to Fig. 5 for notation.

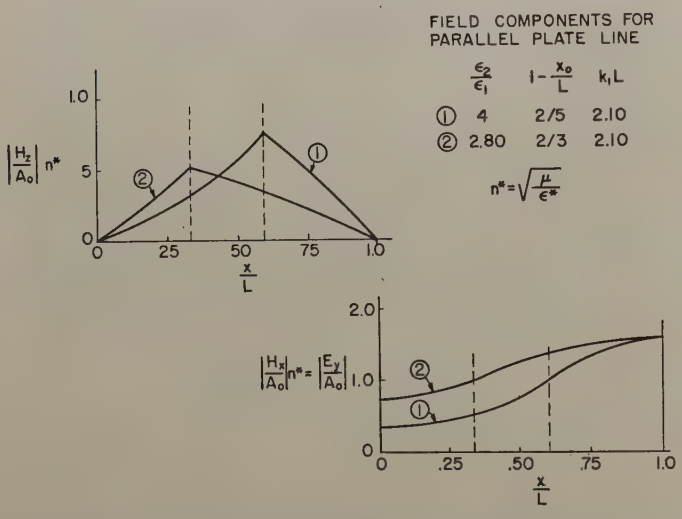

Fig. 7—Field components for composite parallel plate transmission lines. Refer to Fig. 5 for notation.

The results of this section may be summarized as follows. The transverse electromagnetic wave cannot be propagated for $k_1 \neq k_2$. The principal wave is of transverse electric type, and the effective dielectric constant for the principal wave depends upon frequency as well as upon line parameters. At very low frequencies the effective dielectric constant is given approximately by an electrostatic capacity calculation. The higher order modes are of transverse electric type or of a combination transverse electric transverse magnetic type.

The Composite Coaxial Line

The problem considered here is that of the determination of permissible wave types in a coaxial transmission line filled with two different lossless dielectrics with the surface of discontinuity being a circular cylinder concentric with the perfectly conducting cylinders which form the boundary of the transmission line. A cross section of the transmission line is shown in Fig. 8 with the Z axis directed out of the paper.

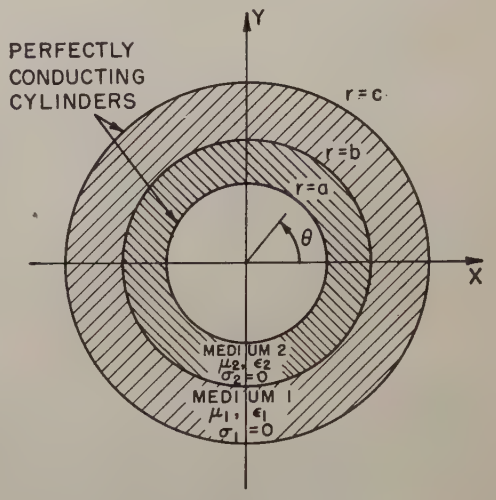

Fig. 8—Composite coaxial transmission line.

The analysis of this configuration is very similar to that for the configuration of Fig. 1 with the wave functions of circular cylindrical co-ordinates being used in place of those of rectangular co-ordinates. It will not be produced in detail, but the results for the principal wave will be indicated.

The principal wave is cylindrically symmetrical and is of the transverse magnetic type. It is convenient to use the following symbols:

$$\begin{aligned} \rho &= \sqrt{h^2 - k_1^2}\,r, & R &= \sqrt{k_2^2 - h^2}\,r, \\ \beta &= \sqrt{h^2 - k_1^2}\,b, & B &= \sqrt{k_2^2 - h^2}\,b, \\ \gamma &= \sqrt{h^2 - k_1^2}\,c, & A &= \sqrt{k_2^2 - h^2}\,a. \end{aligned} \tag{43}$$

The equation which permits determination of the effective dielectric constant of the principal wave is

$$\frac{K_0(\gamma)I_0(\beta) - K_0(\beta)I_0(\gamma)}{K_0(\gamma)I_1(\beta) + K_1(\beta)I_0(\gamma)} = \frac{\epsilon_1}{\epsilon_2}\sqrt{\frac{k_2^2 - h^2}{h^2 - k_1^2}}\,\frac{N_0(A)J_0(B) - J_0(A)N_0(B)}{N_0(A)J_1(B) - J_0(A)N_1(B)}. \tag{44}$$

Low frequency solutions of (44) may be approximated by using the following approximate expressions for the Bessel functions which are valid for small arguments:

$$J_0(z) \simeq 1, \qquad J(z) \simeq \frac{z}{2},$$

$$I_0(z) \simeq 1, \qquad I_1(z) \simeq \frac{z}{2},$$
$$N_0(z) \simeq \frac{2}{\pi} \log z, \qquad N_1(z) \simeq -\frac{2}{\pi z}, \tag{45}$$
$$K_0(z) \simeq -\log z, \quad \text{and} \quad K_1(z) \simeq \frac{1}{z}.$$

With these substitutions

$$\epsilon^* \simeq \epsilon_1\epsilon_2 \frac{\log\left(\frac{c}{a}\right)}{\epsilon_2 \log\left(\frac{c}{b}\right) + \epsilon_1 \log\left(\frac{b}{a}\right)} \tag{46}$$

is obtained. This is exactly the value of ϵ^* that would be predicted on the basis of a calculation of electrostatic capacity.

The higher order modes for this configuration are of transverse electric type, transverse magnetic type, and a combination transverse electric transverse magnetic type.

Conclusions

Three types of composite transmission lines have been analyzed. Of the wave types that can be propagated in these transmission lines, one in each case can be propagated at all positive frequencies. These are the principal waves upon which attention has been focused in this paper.

Transcendental equations, the solution of which will permit the determination of operating characteristics, have been obtained for each transmission line type. For the principal wave the results have been presented in terms of an effective dielectric constant. At low frequencies this effective dielectric constant approaches the value that would be obtained on the basis of an electrostatic capacity calculation.

Equations which permit the determination of the cut-off frequencies for higher order modes have been obtained for each transmission line analyzed. These cut-off frequencies are generally between those that would be obtained if the line were entirely filled with one material or the other.

Arrays of Closely-Spaced Nonresonant Slots*

R. J. STEGEN†, ASSOCIATE, IRE, AND R. H. REED‡, ASSOCIATE, IRE

Summary—**Slots laid broadside to each other exhibit mutual coupling of such magnitude that the design of practical linear arrays of such slots has hitherto been difficult, if not impossible. The technique presented here will produce arrays capable of generating pencil beams or shaped beams with controllable side-lobe level. A large number of slots per wavelength are used and the mutual-coupling effects are kept small by making the slots short compared to a half wavelength. Tests have shown that these arrays may be placed side by side without interaction, thus making it possible to construct a two-dimensional array.**

Introduction

THE ADVENT of high-speed aircraft has made imperative the use of flush-mounted antennas. Although small and relatively omnidirectional antennas of this type exist, flush antennas that would be suitable for radar applications are necessarily large compared to wavelength, and present some serious problems. To date the study of large antennas capable of being flush-mounted has proceeded along two principal lines: *a*. surface-guided wave antennas and *b*. two-dimensional resonant slot arrays. Surface-guided wave antennas, complicated by the necessity of combining transmission line and radiator into a single device, are inherently end-fire. The design of conventional two-dimensional slot arrays leads to mutual-coupling problems of such magnitude as virtually to prohibit usable designs. The arrays of closely-spaced nonresonant slots to be discussed demonstrate a practical method for the design of an extremely broadband antenna with characacteristics intermediate between surface-wave and broadside slot antennas.

Resonant Slot Arrays

A study was initiated whose object was to produce a $\csc^2 \theta \pm 3$ db radiation pattern from 10 to 45 degrees with a side-lobe level 20 db or better below the main beam. The polarization was to be vertical, and the antenna was to operate in *L*-band over a frequency band of ± 12 per cent. The pattern was to be obtained by means of a uniform array of slots placed on a curved surface ten wavelengths long. Several of these arrays were then to be placed side by side to form a two-dimensional array with a narrow azimuth beam. Each linear array would consist of slots series-coupled to a sandwich strip TEM line traveling-wave feed, the coupling being adjusted by varying the lateral distance between the slot centers and the center conductor. The traveling-wave feed would be terminated in the usual matched load. Since this arrangement would make the broad sides of the slots adjacent, it would represent the condition of maximum mutual coupling.

* Original manuscript received by the PGAP, October 14, 1953; revised manuscript received, March 2, 1954.

† Formerly with Hughes Research and Development Laboratories, Culver City, Calif., now with Canoga Corporation, Van Nuys, Calif.

‡ Hughes Research and Development Laboratories, Culver City, Calif.

The shape of the linear array was calculated using a modification of the principle of stationary phase[1] which resulted in the curve shown in Fig. 1. The figure also shows a straight-line approximation to the curve which was made to facilitate construction. This approximation represents a maximum phase error of ±15 degrees,

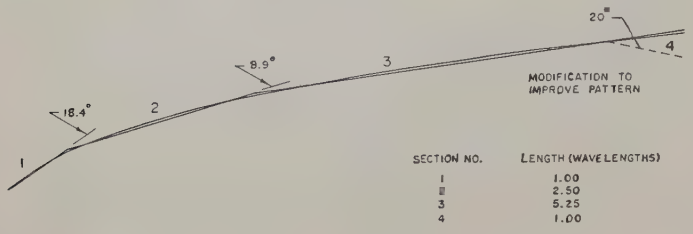

Fig. 1—Straight-section approximation to calculated curve.

which should cause no difficulty. The radiation pattern of this surface was calculated assuming a continuous distribution with a phase constant of 0.899 relative to free space. This phase constant was designed to place the main beam at $\theta = \cos^{-1} 0.899 = 26$ degrees from end-fire with respect to the longest section of the array. This longest portion of the array would therefore be tilted 26 degrees with respect to the horizon to permit the beam to have a cosecant squared pattern from 10 to 45 degrees. The calculated radiation pattern is shown in Fig. 2.

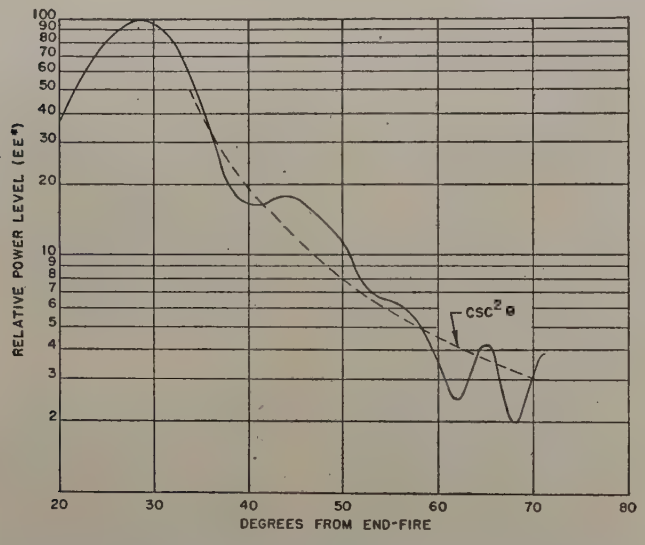

Fig. 2—Calculated radiation pattern of four-section modified surface.

A linear array shaped as the modified surface of Fig. 1 was constructed using resonant slots spaced a quarter wavelength apart. The maximum width of the strip TEM line is restricted by higher-order modes, so the slot length was limited to a quarter wavelength, resonance being achieved by means of dielectric loading. Series-capacity loading was used to reduce the propagation constant in the feed line to 0.899, the value used in the theoretical pattern calculation. The measured radiation pattern of this uniform array was poor, having deep nulls in the shaped portion of the beam, and high side-lobes elsewhere. Some improvement could be obtained over a narrow band through experimental adjustment of the slot couplings. The failure of this array was attributed to phase errors caused by mutual-coupling effects.

Tests were performed on arrays having different slot spacings, and it was noted that the arrays having the closest slot spacings produced the best radiation patterns. It appeared that further improvement might be obtained through an appreciable increase in the number of slots per wavelength.

Nonresonant Slot Arrays

The slot coupling is necessarily low in a traveling-wave feed having a large number of elements. In the desired array it was found advantageous to use nonresonant slots in order to ease the close tolerances required by low coupling. The coupling of a nonresonant slot is easily adjusted by varying the slot length and, though the reactances of such slots are greater than their resistances, in a large array these reactances generally cancel each other. In a large array these reactances are so small that their effect upon the phase constant of the transmission line is negligible. Since the phase of radiation of nonresonant slots is relatively insensitive to frequency, the use of such slots should improve broadbanding.

The measured radiation pattern of a uniform array containing sixteen nonresonant slots per wavelength is shown in Fig. 3. A reasonably satisfactory $\csc^2 \theta$ pattern and a −21 db side-lobe level were obtainable. Because this number of slots does not represent the limiting case, (i.e., the slots are still rather widely separated), it appeared that further improvement might still be possible.

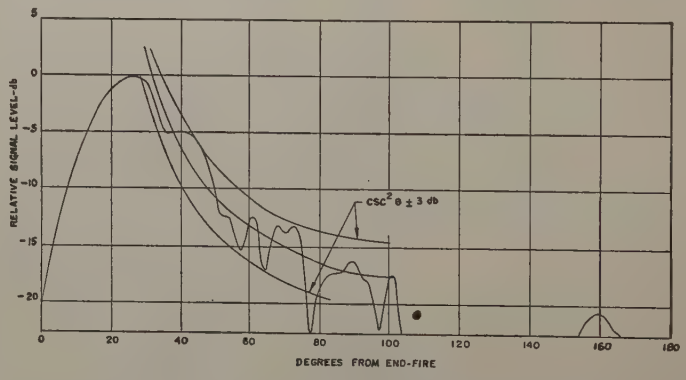

Fig. 3—Measured radiation pattern of uniform array having 16 slots per wavelength.

The number of slots per wavelength was increased to thirty-six. This was accomplished by placing wires across an open broad face of the strip TEM line as

[1] S. Silver, "Microwave Antenna Theory and Design," McGraw-Hill Book Co., Inc., New York, N. Y., pp. 119–122; 1949.

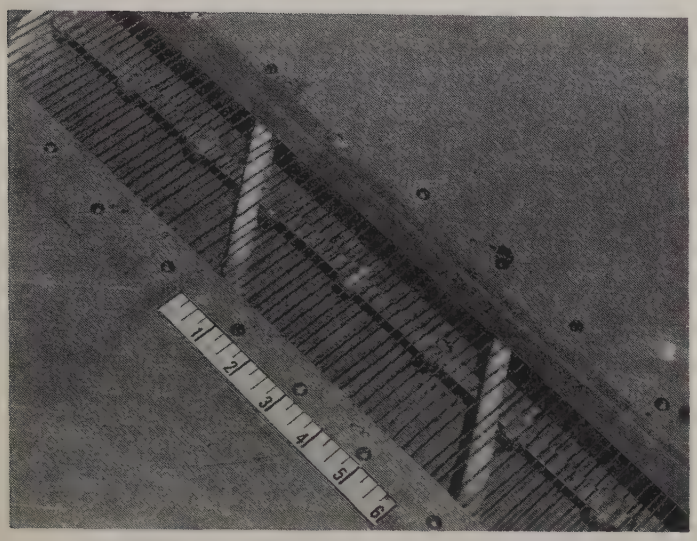

Fig. 4—Detail of array with 36 slots per wavelength.

shown in Fig. 4. Small ground planes were placed on either side of the array to reduce scattering in the low side-lobe regions. The lengths of the slots were found to be easily controlled by partially covering them with metallic tape. Fig. 5 shows the radiation pattern of this uniform array. As can be seen, the beam is within $\csc^2 \theta \pm 3$ db out to 52 degrees from the main beam, with some coverage to 85 degrees. The side-lobe level is below -24 db. Agreement with the calculated pattern is reasonably good considering the experimental difficulty of obtaining an accurate uniform illumination.

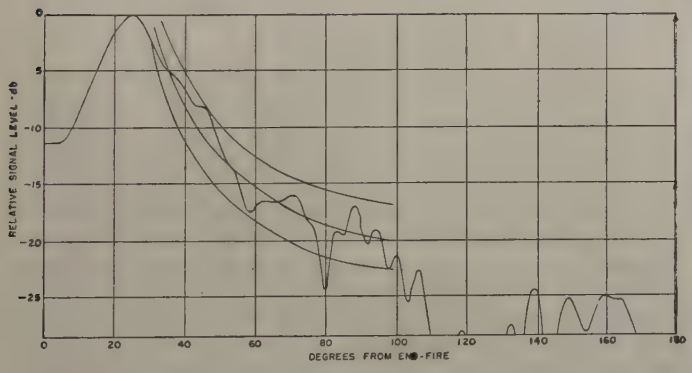

Fig. 5—Radiation pattern of uniform array having 36 slots per wavelength.

Two arrays fed by a simple tee junction were tested side-by-side. The spacing between the arrays was 1.14 wavelengths, but the results of the investigation indicate that the arrays could have been separated by less than a wavelength without adverse effect due to mutual coupling. A spacing greater than one wavelength is permissible in this particular antenna because of the rather narrow azimuth beam of each linear array. The patterns obtained with the arrays fed singly and jointly are shown in Fig. 6. The patterns of the individual arrays are not identical due to the difficulty of obtaining accurate slot excitations; nevertheless, the patterns of the two arrays fed jointly is very closely the sum of the individual patterns. In an additional test, the power received by one array when the other was fed was found to be down 38 db. It can therefore be concluded that the two arrays interact negligibly. This immediately implies that a two-dimensional array can be built having a narrow beam in azimuth and a $\csc^2 \theta \pm 3$-db pattern in elevation.

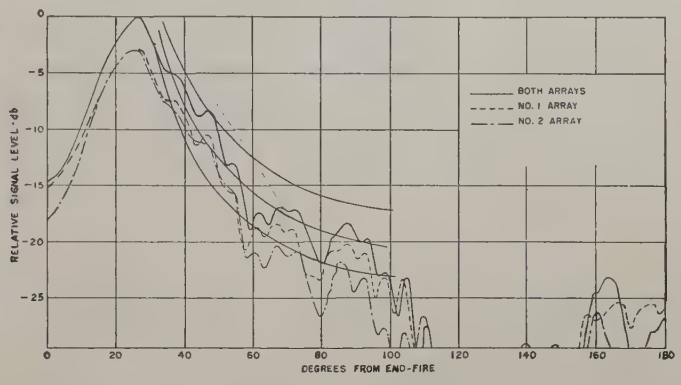

Fig. 6—Comparison of arrays fed single and side by side.

A two-dimensional array consisting of three of the described linear arrays fed in equal amplitude and phase was built and tested. A photograph of this array is shown in Fig. 7. Radiation patterns as a function of frequency are given in Figs. 8, 9, and 10. The $\csc^2 \theta \pm 3$-db pattern and -21 db side-lobe level could be held over a ± 15 per cent band provided the over-all shift in beam position is taken into account. The increase in beamwidth at the highest frequency is caused by a decrease of phase velocity in the TEM line which moves the main beam closer to end-fire. This decrease in phase velocity at higher frequencies is a natural consequence of a lower reactance in the series capacity loading.

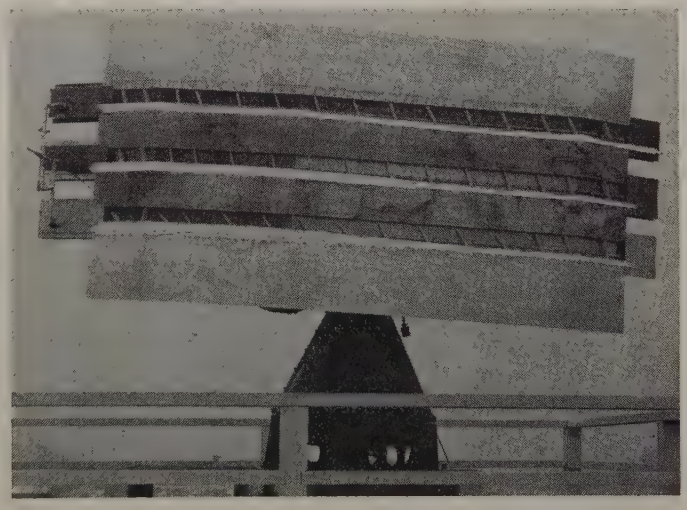

Fig. 7—Triple array with 36 slots per wavelength.

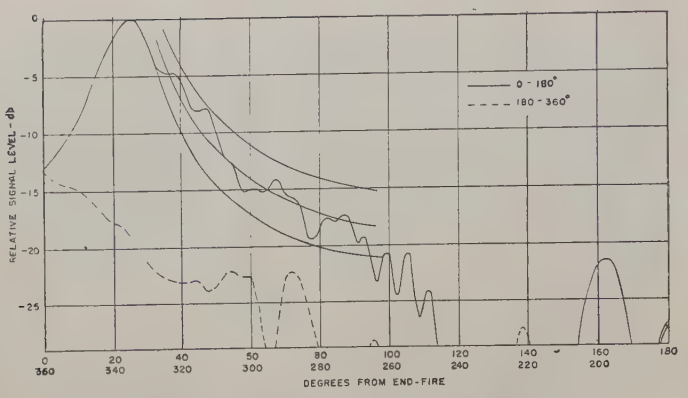

Fig. 8—Radiation pattern of triple array at design frequency.

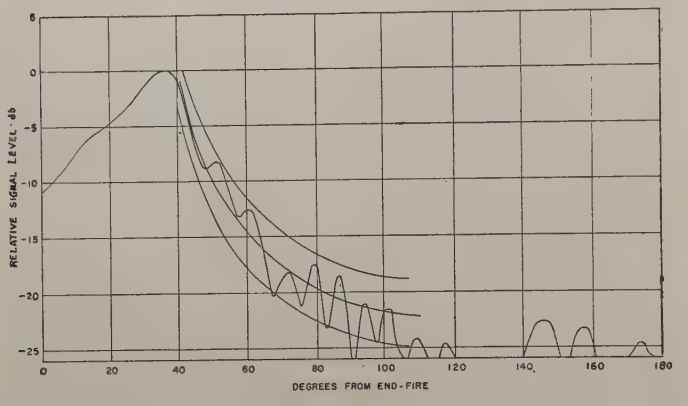

Fig. 9—Radiation pattern of triple array at 15.4 per cent below design frequency.

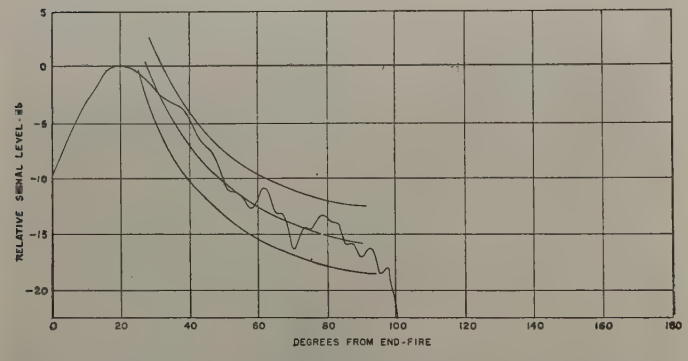

Fig. 10—Radiation pattern of triple array at 11.5 per cent above design frequency.

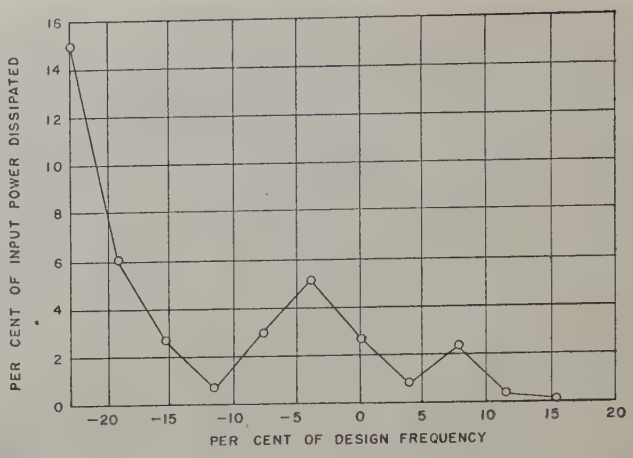

Fig. 11—Per cent of input power lost in matched termination.

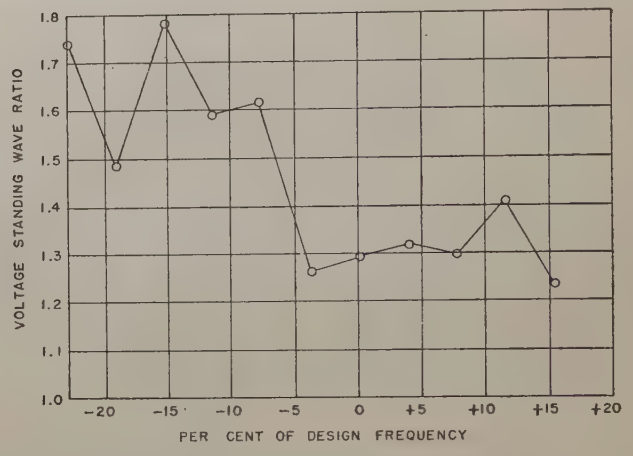

Fig. 12—Input vswr of array vs frequency.

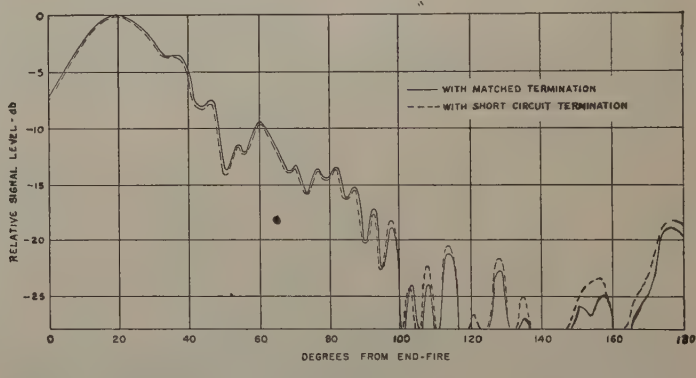

Fig. 13—Comparison of radiation patterns with matched and short-circuit terminations at $f = 11.5$ per cent above design frequency.

Measurements were performed on a single linear array to determine the input voltage standing-wave ratio and the per cent power into the terminating load. The results are plotted in Figs. 11 and 12. The per cent power into the load was determined by means of relative power measurements at both ends of the array, and is under 6 per cent over the frequency band within which the antenna has a −21-db side-lobe level. Since the power into the load is very small at some frequencies, the results were checked by an alternate method. This method consisted of replacing the matched termination with a short circuit and observing the change in the radiation pattern. If the power into the load is high, a short-circuit termination should, in this specific design, result in a great deal of radiation in the region of low side-lobe level. Checks performed by this method corroborated the previous measurements. As an example, two patterns, one obtained with a matched load and one with a short-circuit termination, are compared in Fig. 13. The frequency chosen was 11.5 per cent above

the design frequency, since this is a point of indicated high efficiency. Variations in the pattern are under ±1 db at the −24-db level, showing that the power into the load is no higher than the measured 0.4 per cent.

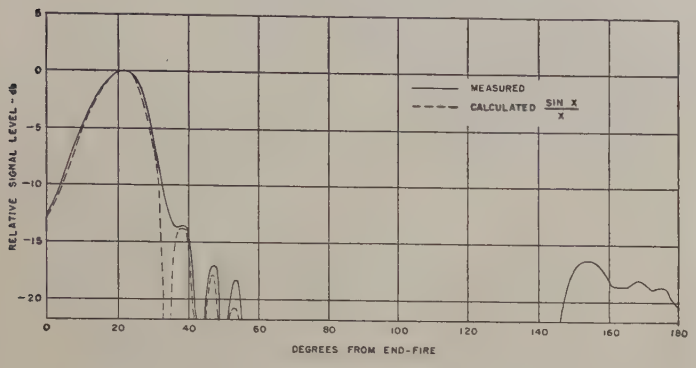

Fig. 14—Radiation pattern of uniform rectilinear array.

A uniform rectilinear array having 36 nonresonant slots per wavelength was constructed and tested for comparison with the theoretical pattern. The radiation pattern of this array is shown in Fig. 14, along with a calculated $(\sin x)/x$ (uniform array) pattern. Discrepancies exist, the greatest one being absence of the first null. Nevertheless, considering the experimental difficulties of adjusting for an accurate uniform distribution, a reasonable pattern seems to have been obtained.

Conclusion

In conclusion, it may be stated that through the use of a large number of nonresonant slots per wavelength, linear arrays may be built which, under conditions of strong mutual coupling between slots, will give the radiation pattern calculated for a continuous distribution. The aperture distribution of these arrays is easily controlled, and the main beam may be directed anywhere except in the immediate vicinity of broadside. Such arrays, once designed, may be placed side by side without affecting their array factors, thus permitting the construction of two-dimensional flush antennas.

Acknowledgment

The authors wish to thank Dr. L. C. Van Atta for suggesting the curved surface, I. K. Williams for suggesting the wire approach to the array construction, and I. P. Kaminow for assisting in the measurements and in the preparation of this paper.

A New Antenna Feed Having Equal *E*- and *H*-Plane Patterns*

ALVIN CHLAVIN†, ASSOCIATE, IRE

Summary—**When two complementary sources are combined in the proper amplitude and phase, desirable radiation characteristics for feeding a circular aperture are obtained. It is shown that when the feed is achieved there results a circular beam cross section which optimizes the efficiency of illumination of a circular aperture. The back radiation from the feed is down 30 db from that in the forward direction, minimizing interference effects between feed and aperture. It is the purpose of this thesis to show how a feed composed of complementary sources has been physically realized and to present and discuss experimental radiation and impedance data.**

It is well known that the radiation pattern of an electric dipole is a circle in the *H* plane and a figure 8 in the *E* plane. An open-ended coaxial line carrying the TE_{11} mode is similar to a magnetic dipole; i.e., the *E* plane is nearly circular while the *H* plane is like a figure 8. These two sources have been combined to produce a feed whose *E*- and *H*-plane patterns are of equal width.

The complementary source idea has been applied to feeds of both linear and circular polarization. The linearly polarized feed is excited from rectangular waveguide and is simple to fabricate. It can be easily matched over a broadband. This feed has been used to illuminate a 20-inch parabola with the result that the secondary *E* and *H* planes are of equal width and the side lobes are 30 db down from the main radiation. The circularly polarized feed is excited from a circularly polarized TE_{11} mode in coaxial line. The radiating structure maintains circular symmetry and the axial ratio remains essentially constant over a large portion of the beam.

* Original manuscript received by the PGAP, September 15, 1953; revised manuscript received, April 15, 1954.

† Hughes Aircraft Co., Culver City, Calif.

Introduction

IN DEALING WITH pencil-beam radiation patterns derived from circular paraboloids, the antenna designer tries to maintain certain performance characteristics constant with frequency. Important ones of these characteristics are the relative intensity of the side lobes, the gain, the voltage standing-wave ratio, and, for conically scanning radars, the level of the cross-over point. The designer desires to maintain the gain high and the side and cross-polarization lobes low. To obtain these results the parabola must be properly fed.

It will be shown that if a feed composed of two complementary sources of equal amplitude are combined in the proper phase the resulting radiation pattern will be identical in the *E* and *H* planes, and furthermore, the back radiation for the combination will be zero. If such a feed having a circular beam cross section is used to illuminate a circular paraboloid, an antenna system of high efficiency will result since the feed has an axially symmetric illumination.[1] The secondary radiation will have a circular beam cross section, moreover, the gain

[1] J. D. Lawson, "The practical aspects of paraboloid aerial design," *Jour. IEE*, vol. 93 IIIA, pp. 1511–1522; 1946.

and side lobes will be little affected by frequency changes because of the low back radiation from this feed. An additional advantage is gained by the reduction of cross-polarization lobes since it has been shown that a feed composed of complementary sources will minimize this effect.[2] Theoretically, if the amplitudes and phases of the complementary sources are properly chosen the cross-polarized lobes will have zero amplitude.

It is the purpose of this paper to show how a feed composed of complementary sources can be physically realized, and to present the radiation patterns and impedance data obtained. A feed of this type would find wide application when used in a conically-scanning radar since the cross-over point is of constant level with respect to the height of the main beam as the paraboloid rotates.

The Feed Design

The feed consists of two sources which have complementary types of radiation characteristics orientated at right angles to one another. These two radiation sources are an electric dipole and the open end of the coaxial line carrying the TE_{11} mode. Each of these sources has in the past been used as a feed in its own right.[3] The discussion that follows describes just how these two sources are combined to form the new feed.

It is well known that the pattern of a dipole is a circle in the H plane and a figure 8 in the E plane. If a half-wave-diameter disk is placed perpendicular to the feed line about a quarter-wavelength away as a reflector, back radiation is decreased about eight db with respect to forward radiation but the broad H-plane and relatively narrow E-plane patterns still persist.

On the other hand, the open end of a waveguide or a coaxial line carrying the TE_{11} mode has a pattern that is nearly the complement of that of an electric dipole if the diameter of the waveguide is less than one wavelength. That is, the E-plane pattern is almost a circle and the H-plane pattern is almost a figure 8. This type of feed usually is used in conjunction with a splash plate which directs the energy back at the paraboloid.

Since these two sources have patterns of complementary characteristics, it was considered possible to combine them in such a manner as to have one compensate the other so that equal beamwidths would be obtained. Fig. 1(a) shows schematically how the field patterns of two complementary sources would appear. There is an electric and a magnetic dipole separated by a distance X, and for simplicity the fields are drawn as if they originated from the center of the two sources. The symbol E represents the radiation-field intensity, the superscript indicates whether it is the electric or the magnetic dipole that is radiating, and the subscript indicates if it is the electric- or magnetic-radiation planes.

[2] E. M. T. Jones, "Low side lobes in pencil-beam antennas," Convention Record of the IRE, 1953, National Convention, Part 2—Antennas and Communications.

[3] S. Silver, "Microwave Antenna Theory and Design," vol. 12, M.I.T. Radiation Laboratory Series, Sections 8.8 and 10.4, McGraw-Hill Book Co., Inc., New York, N. Y.; 1949.

Fig. 1(*b*) is a photograph of a feed used for test purposes that was built using rectangular X-band waveguide. The narrow dimension of the waveguide was reduced and a hole was drilled through the broad face of the guide in this narrow region and a bead-supported dipole then centered in the hole. This now represents the dipole source. The TE_{11} source was obtained by placing a metallic cylinder around the waveguide in the region of the dipole. The cylinder and the feed line form a coaxial line with a rectangular center conductor.

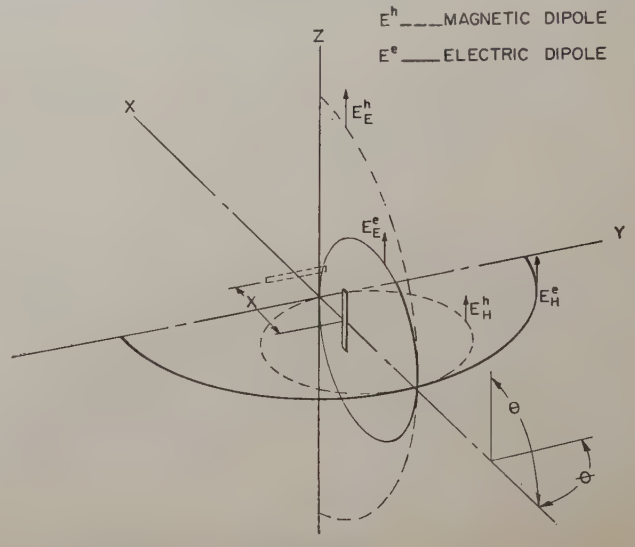

(a)

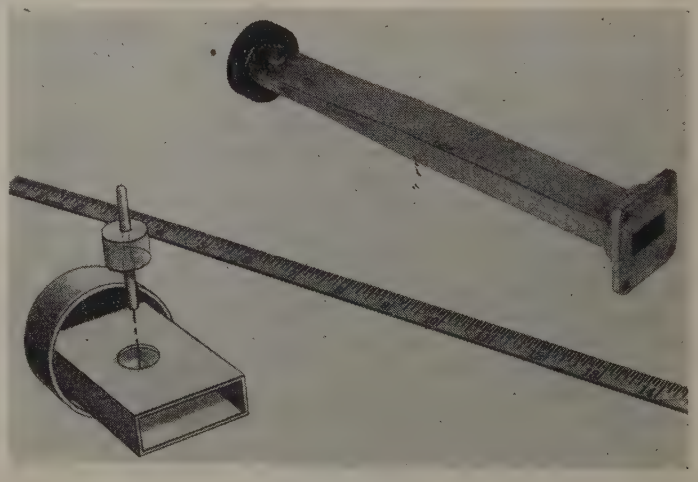

(b)

Fig. 1—(a) Electric- and magnetic-field distributions for two complementary dipole sources. (b) Test feed.

The dipole excites parasitically a TE_{11} mode in this irregular coaxial line which is terminated in a short circuit placed behind the dipole and is left open on the other end. This open aperture is the TE_{11} source.

If the cylinder is very long it will completely surround the dipole and only the TE_{11} source will radiate with its broad E- and narrow H-plane patterns. If the cylinder is shortened until the dipole is exposed, its radiation will no longer be confined to the inside of the cylinder, but will be free to spill out into the exterior region with

its own pattern now adding to that of the TE_{11} source. If the cylinder is reduced in length to the extreme of only the metal short circuit remaining, there is only the disk-dipole source with its broad H- and narrow E-plane pattern left. It follows, then, that at some length between the extremes of a very long cylinder and a zero-length cylinder the patterns should be of equal width. This turns out to be the case. It also turns out that when the E- and H-plane patterns are made equal, the back radiation from the feed is a minimum. Proof of this is shown in the Appendix.

It should be pointed out that the exact length of the cylinder for equal E- and H-plane patterns is a function of the distance from the cylinder short to the dipole. That is, when the short is far from the dipole the cylinder must be longer than when the short is close to the dipole. This presents a means for controlling the beamwidth of the feed as the beamwidth is narrower for close spacings than for more remote spacings of the short. The beamwidth also may be controlled by means of the cylinder diameter, with a smaller cylinder having a broader beam than a large cylinder. In all cases, the back radiation is lowest when the E and H planes are equal and is lower for close short spacings than for greater spacings.

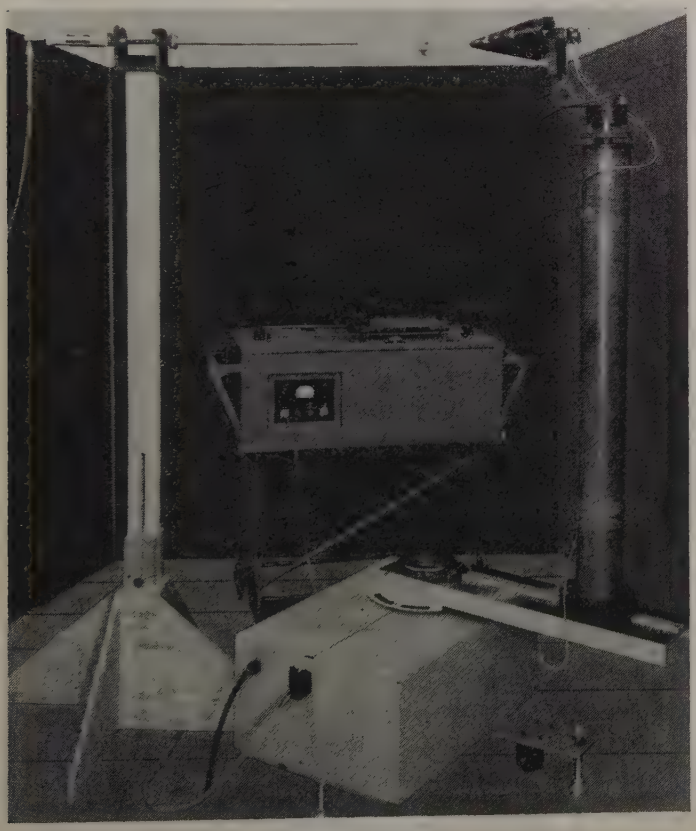

Fig. 2—Primary pattern range.

Pattern Measurements

The primary patterns of the feed were obtained on the specially built range shown in Fig. 2. The feed is used as a receiver and is mounted on a phenolic mast which is attached to a slowly rotating steel beam. There are two servo motors which monitor the motion of the beam, and drive a table on the automatic pattern recorder such that a range of 180 or 360 degrees may be recorded. The transmitter is an open-ended rectangular guide that has been matched with an iris.

An interesting addition to the pattern range is the use of an X-band Z_0 cloth cone around the feed near the mounting flange. Reflections from this flange produced a scattered field which resulted in an undesirable fine structure on the pattern. The use of the absorbing cone almost completely eliminates this effect. The entire pattern range is surrounded with absorbing materials for elimination of stray reflections. Both the transmitter and receiver can be rotated so that either the E or H plane can be measured.

The secondary patterns of Figs. 6 and 7 were measured with the same type recorder on an outdoor range of sufficient separation to insure far zone patterns. The mountings also were arranged so that either the E- or H-plane patterns could be taken.

Figs. 3(a) to (d), p. 116, show primary pattern development of the feed as a function of the cup cylinder length. These patterns are for a cylinder diameter of slightly more than one inch, which is just sufficient to place over the rectangular section of guide. In Fig. 3(a), the cylinder is of zero length with the short being 0.313 inch from the dipole. The result is a typical dipole pattern of broad H- and narrow E-plane patterns. Note that the back radiation is about nine db down. Fig. 3(b) shows what occurs when the cylinder is lengthened so that it extends 0.150 inch beyond the short. Here the H plane has narrowed, the E plane has broadened and the back radiation decreased to a level of about 17 db. Fig. 3(c) shows the pattern in which the cylinder length is increased to 0.225 inch. With this length the E and H planes are almost equal, and the back lobe is down about 18 db from the peak. The dipole is still slightly exposed, however. In Fig. 3(d) the dipole is covered as the cylinder is lengthened to 0.350 inch. The E plane is now broader than the H plane and the back-lobe level is slightly higher at 15 db down.

Fig. 4, page 116, shows a pattern obtained with a slightly larger cylinder diameter (1.450 inch O.D.). E- and H-plane patterns are equal with a beamwidth of about 65 degrees at the 10-db point. The back radiation is about 30 db down; in fact, for the back ± 60 degrees the radiation is below 20 db.

Fig. 5, page 116, shows effect of changing cylinder length on E- and H-plane beamwidths. There are two E-plane and two H-plane curves shown, each one representing a different short location of the cylinder. These data are for the 1.450-inch O.D. cylinder diameter used to obtain the radiation pattern of Fig. 4. It should be observed that there exists a large range of bandwidths for which one may obtained E- and H-plane patterns.

Measurements were made to determine the characteristics of the secondary cross-over patterns obtained with

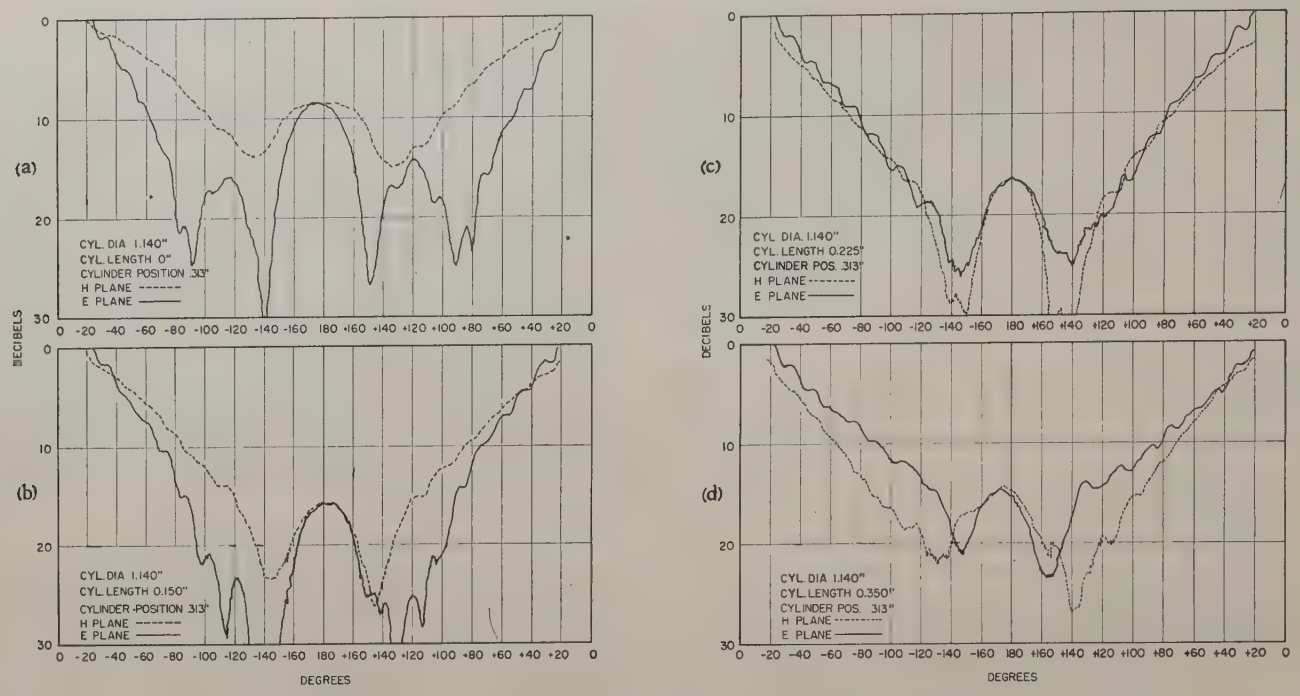

Fig. 3—Effect of cylinder length on beamwidths and back lobe.

a 20.75-inch paraboloid reflector with an f/d ratio of 1/3 and an offset of 1.25 degrees. Fig. 6 shows the results of these measurements. The three patterns were taken over a frequency band of 400 megacycles. Note the equality of the E- and H-plane patterns and the constant height of the side lobes. The cross-over level is constant and the same in both planes. The side lobes are of the order of 30 db down exterior to the swept area of the beam.

In Fig. 7(a) and (b) are shown patterns at the ends of an even larger frequency band, the former being taken at 8,400 mc and the latter at 9,600 mc. At these extremes the cross-over level has risen about 0.25 db and the side lobes are about 26 db down. It will be noted, however, that the E and H planes are still of equal widths. The gain of this paraboloid was measured and found to be 31.7 db at 9,000 mc, which shows an efficiency of nearly 65 per cent.

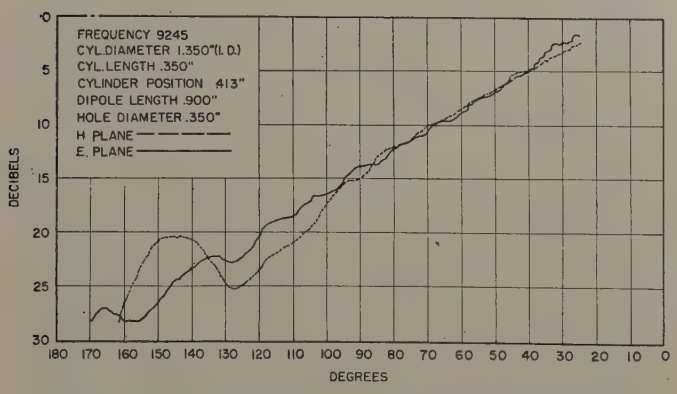

Fig. 4—Typical primary pattern obtainable with a one-wavelength-diameter cylinder.

Impedance

The impedance of the feed is dependent upon the cylinder position, the position of the waveguide short behind the dipole, the length and diameter of the dipole as well as the dipole supporting mechanism, and the hole diameter through which the dipole protrudes. Unfortunately, these same parameters affect the power at which breakdown occurs in the feed. Since the cylinder length and position are fixed by pattern requirements, they cannot be used as parameters in the impedance matching.

The problem of adjusting the parameters reduces itself to obtaining the largest power with the greatest bandwidth. The larger the hole diameter the less chance for arcing across the guide to the dipole. With a 0.450-inch diameter hole and a short teflon bead just resting in the hole on shoulder, the feed transmitted 120 kw

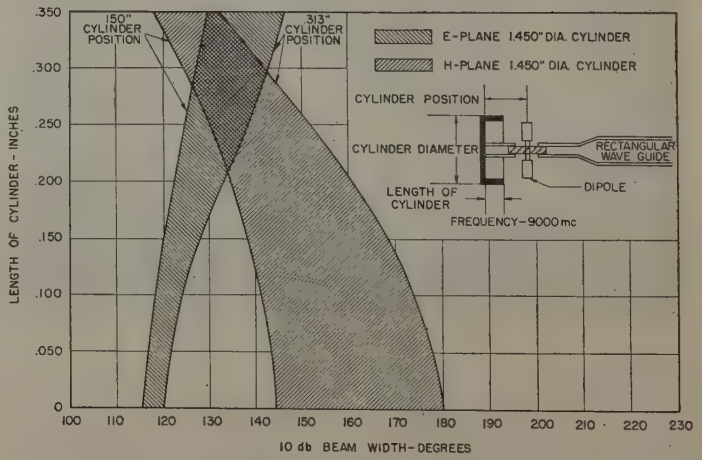

Fig. 5—Effect of cylinder length and position on the E- and H-plane beamwidths.

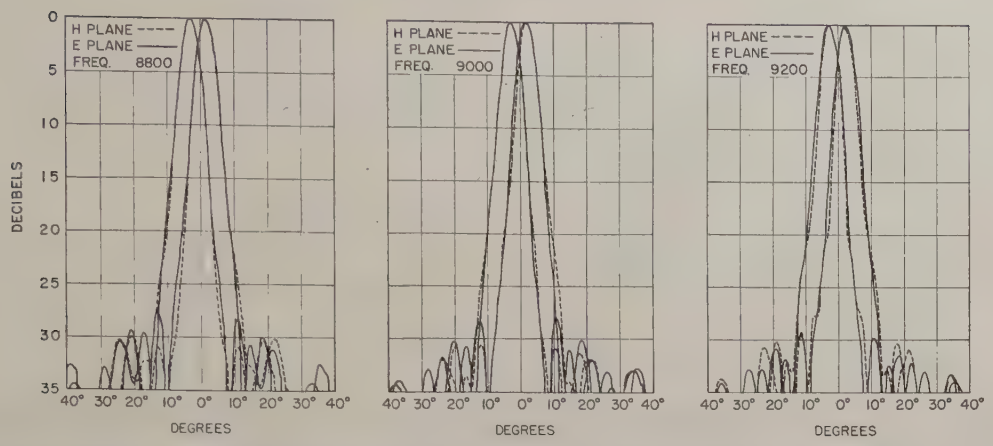

Fig. 6—Secondary patterns obtained at different frequencies with a 20.75-inch diameter paraboloid with an f/d of 1/3. Paraboloid offset 1.25 degrees to show constant height of the cross-over point relative to height of main beam.

without arcing. The frequency bandwidth in this condition was about two per cent under a vswr of 1.5.

When the hole diameter was reduced to 0.350 inch, the bandwidth improved considerably. Fig. 8 is a curve of vswr as a function of frequency for this hole diameter. A bandwidth of 11 per cent with a vswr under 1.5 was obtained. The supporting mechanism was a round bead pushed into the narrow region of the waveguide. The diameter of the bead affects the match, the optimum size being about 0.500 inch for teflon. The power at which breakdown occurs for this condition is about 75 kw. A bandwidth of 22 per cent was obtained for a hole diameter of 0.250-inch and 0.500-inch teflon bead; however, the power-handling ability for this condition is below 50 kw.

The impedance data taken were of the feed itself without a paraboloid. The parabola will introduce a reflection into the feed which causes the vswr to fluctuate rapidly with frequency changes. This problem is common and is discussed in the literature.[4] Vertex plates may be used to reduce the reflections at the expense of pattern deterioration.

[4] A. V. Peppard and N. Elson, "The elimination of standing waves in aerials employing paraboloidal reflectors," *Jour. IEE*, vol. 93 IIIA, pp. 1531–1535; 1946.

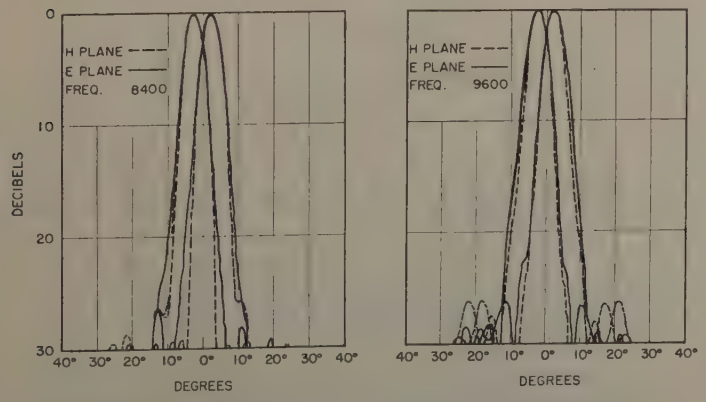

Fig. 7—Secondary patterns of the extremes of an 8,400- to 9,600-mc band for the paraboloid of Fig. 6.

Circular Polarization

Circular polarization with this type of feed is limited to low-power applications. A feed may be constructed out of round waveguide carrying the TE_{11} mode. Instead of one pair of holes, two are introduced at right angles to each other in the same plane. Equal length dipoles are placed through these holes and result in a symmetric cross. Behind this cross a cylinder is placed of the proper length and in the proper position. A quarter-wave plate is introduced in the line preceding the cross and the feed is complete.

The difficulty with such a construction is that the waveguide diameter must be kept less than $\lambda_0/2$ or the dipoles will be separated by too great a distance and the H plane will become too narrow. This means that the waveguide should be dielectric loaded to reduce the diameter. Feeds of this type have been built and the axial ratio of the polarization over the main beam remains less than one db until the first null is approached. However, because of the dielectric loading, their application lies in very low power work.

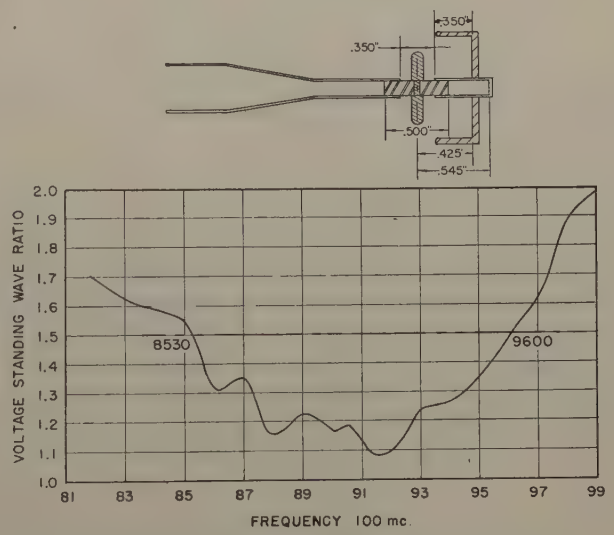

Fig. 8—Vswr as a function of frequency for a 0.350-inch diameter hole.

Conclusion

1. A feed having equal E- and H-plane patterns over a 12-per cent band can be obtained by the proper combination of the dipole and a TE_{11} source.
2. The back radiation from this feed is as much as 30 db down.
3. Bandwidths of 22 per cent with a vswr under 1.5 can be obtained for low-power-handling capacity feeds.
4. Power-handling ability of 120 kw is possible at sea level.
5. Circular paraboloid efficiencies approaching 65 per cent can be obtained.
6. Cross-polarization lobes are minimized.

Acknowledgment

The experimental work involved in this thesis was performed at the Hughes Aircraft Company Research and Development Laboratories by special arrangement with the College of Engineering of the University of California at Los Angeles. Acknowledgments are made to Professor W. D. Hershberger, Chairman of the Masters Thesis Committee, for his interest and guidance, to T. T. Taylor for his suggested use of the TE_{11} coaxial line mode, and to R. T. Teragawa for his laboratory aid.

Appendix

The proof that the front-to-back ratio, of a feed composed of complementary sources, is a maximum when the E- and H-plane patterns are made equal is shown below. Let E_E be the radiated field in the E plane and E_H be the radiated field in the H plane. A_1 and A_2 are the amplitudes of sources 1 and 2 and $F(\theta)$ or $F(\phi)$ represents the field-pattern function.

Then: for source number one,

$$E_E^{(1)}(\theta) = A_1F_1(\theta) \tag{1a}$$

$$E_H^{(1)}(\phi) = A_1F_2(\phi). \tag{1b}$$

For source number two,

$$E_E^{(2)}(\theta) = A_2F_2(\theta)e^{j\Delta} \tag{2a}$$

$$E_H^{(2)}(\phi) = A_2F_1(\phi)e^{j\Delta}, \tag{2b}$$

where

$$\Delta = \frac{2\pi X}{\lambda}\cos\theta - \psi$$

and X is the separation of the two sources. $\theta = 0$ is the front direction, and $\theta = \pi$ is the back direction. ψ is the phase difference of the two sources. If the sources are complementary, $F_1(\theta) = F_1(\phi)$ and $F_2(\theta) = F_2(\phi)$.

The resultant E- and H-plane patterns are then

$$E_E(\theta) = A_1F_1(\theta) + A_2F_2(\theta)e^{j\Delta} \tag{3}$$

and

$$E_H(\theta) = A_1F_2(\theta) + A_2F_1(\theta)e^{j\Delta}, \tag{4}$$

with absolute values

$$|E_E(\theta)| = |A_1^2F_1^2(\theta) + 2A_1A_2F_1(\theta)F_2(\theta)\cos\Delta + A_2^2F_2^2(\theta)|^{1/2} \tag{5}$$

$$|E_H(\theta)| = |A_1^2F_2^2(\theta) + 2A_1A_2F_1(\theta)F_2(\theta)\cos\Delta + A_2^2F_1^2(\theta)|^{1/2}. \tag{6}$$

It is evident that for

$$|E_E(\theta)| = |E_H(\theta)|,$$

$$A_1^2F_1^2(\theta) + A_2^2F_2^2(\theta) = A_1^2F_2^2(\theta) + A_2^2F_1^2(\theta),$$

or that

$$\gamma = \frac{A_1}{A_2} = 1. \tag{7}$$

It is now necessary to show that the condition expressed by (7) is also necessary for

$$P = \frac{|E_E(\theta)|^2_{\theta=0}}{|E_E(\theta)|^2_{\theta=\pi}} = \text{a maximum}$$

where P = front-to-back ratio.

Remembering that

$$F_1(0) = F_2(0) \quad \text{and} \quad F_1(\pi) = F_2(\pi),$$

then

$$P = \frac{A_1^2F_1^2(0) + 2A_1A_2F_1(0)F_2(0)\cos\Delta_0 + A_2^2F_2^2(0)}{A_1^2F_1^2(\pi) + 2A_1A_2F_1(\pi)F_2(\pi)\cos\Delta_\pi + A_2^2F_2^2(\pi)} \tag{8}$$

$$P = \frac{F_1^2(0)}{F_1^2(\pi)}\cdot\frac{\gamma^2 + 1 + 2\gamma\cos\Delta_0}{\gamma^2 + 1 + 2\gamma\cos\Delta_\pi},$$

where $P_1 = F_1^2(0)/F_1^2(\pi)$ is the power front-to-back ratio of source number one.

Differentiating P with respect to γ and setting equal to zero,

$$\frac{\partial P}{\partial\gamma} = 0 = P_1\left[\frac{2\gamma + 2\cos\Delta_0}{\gamma^2 + 1 + 2\gamma\cos\Delta_\pi} - \frac{(\gamma^2 + 1 + 2\gamma\cos\Delta_0)(2\gamma + 2\cos\Delta_\pi)}{(\gamma^2 + 1 + 2\gamma\cos\Delta_\pi)^2}\right], \tag{9}$$

which simplifies to

$$\gamma^2 = \frac{\cos\Delta_\pi - \cos\Delta_0}{\cos\Delta_\pi - \cos\Delta_0} = 1 \tag{10}$$

or

$$\gamma = \frac{A_1}{A_2} = 1,$$

since -1 has, by definition, no significance.

This is condition (7) above.

That a maximum front-to-back ratio occurs at $\gamma = 1$ is easily seen by taking the second derivative

$$\frac{\partial P}{\partial\gamma} = \frac{2(\gamma^2 - 1)(\cos\Delta_\pi - \cos\Delta_0)}{(\gamma^2 + 1 + 2\gamma\cos\Delta_\pi)}$$

$$\frac{\partial^2 P}{\partial\gamma^2} = \frac{\cos\Delta_\pi - \cos\Delta_0}{(1 + \cos\Delta_\pi)^2} < 0 \tag{11}$$

since

$$\Delta = \delta \cos\theta - \psi$$

$$\Delta_0 = \delta - \psi$$

$$\Delta_\pi = -(\delta + \psi)$$

and

$$\cos\Delta_\pi - \cos\Delta_0 = -2\sin\delta\sin\psi$$

which is negative for δ and ψ, both less than π (i.e., spacing less than $\lambda/2$ and phase difference less than 180 degrees). This is reasonable for an antenna such as the one described.

Hence, the same condition $\gamma = 1$ applies both to equality of the E- and H-plane patterns and to minimum back radiation.

Paraboloid Reflector and Hyperboloid Lens Antennas*

E. M. T. JONES†, ASSOCIATE, IRE

Summary—**A theoretical analysis of the radiating properties of the paraboloid reflector and the hyperboloid lens shows that low amplitude cross-polarized radiation and high gain factors can be obtained from a paraboloid reflector excited by a plane-wave source. Low amplitude, cross-polarized radiation can also be obtained from the hyperboloid lens with a plane-wave feed, but with a lower gain factor. It is found that the measured properties of the antennas agree reasonably well with the theoretical predictions. Also it is found experimentally that principal plane side lobes of the order of —40 db can be obtained with a short focal length hyperboloid lens.**

Introduction

THIS PAPER describes an investigation of the radiation properties of two perfectly focusing devices: the paraboloid reflector and the hyperboloid dielectric lens, excited at their foci by a short electric dipole, a short magnetic dipole, and a plane-wave source. The purpose of this investigation is to examine the radiation characteristics of these antennas, which, at least in the limit of infinitesimal wavelengths, have no phase aberrations in the aperture field. The analysis is divided into two parts: (1) the aperture fields of the two antennas are first computed, and, (2) the far-zone diffraction patterns are then determined. The power gain of the systems is obtained as a by-product of the diffraction pattern computation. Some experimental results are also discussed.

Paraboloid Reflector Aperture Distributions

The aperture distributions of the reflector are computed in two steps. First, the current induced on the surface of the reflector by radiation from the feed is determined. Next, the electric fields in the aperture, arising from these currents, are computed. The assumptions made in the derivation are:

a. The reflector is in the far-zone of the feed, so that only fields varying as the reciprocal of the distance from the feed to the reflector are significant.
b. The feed pattern is the same with the reflector in place as when it is absent.
c. Energy traveling in the region between the reflector aperture and the feed follows the straight line paths predicted by geometric optics, while the polarization of the aperture field is determined by the plane-wave boundary conditions at the reflector surface, namely, that the total tangential electric field in the incident and reflected waves must be zero.

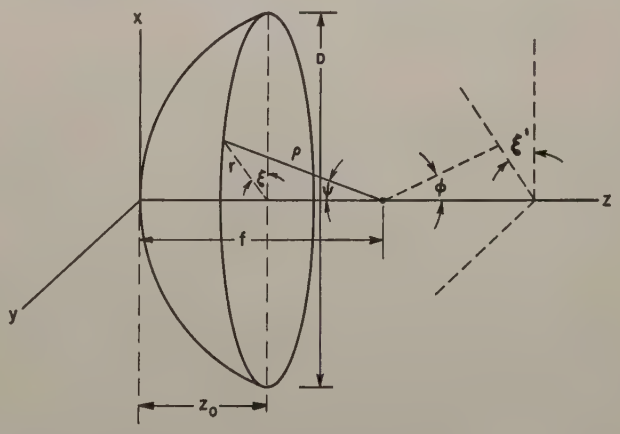

Fig. 1—Sketch of paraboloid reflector illustrating the notation used in the analysis.

A sketch of the parabola showing the notation appears in Fig. 1. The surface current $\overline{K}$ induced on the reflector by the feed at the focus is

$$\overline{K} = 2(\bar{n} \times \overline{H}) = \frac{2}{\eta}\bar{n} \times (\bar{\rho}_0 \times \overline{E})$$

$$= \frac{2}{\eta}\left[\bar{\rho}_0(\bar{n}\cdot\overline{E}) + \overline{E}\cos\frac{\psi}{2}\right], \qquad (1)$$

where

$\overline{E}$ = far-zone electric field of the feed
$\overline{H}$ = far-zone magnetic field of the feed
$\eta = 377$ ohms

* Original manuscript received by the PGAP, November 11, 1953; revised manuscript received April 12, 1954.
† Stanford Research Institute, Stanford, Calif.

and the outward normal $\bar{n}$ to the reflector surface is

$$\bar{n} = -\bar{x}\cos\xi\sin\frac{\psi}{2} - \bar{y}\sin\xi\sin\frac{\psi}{2} + \bar{z}\cos\frac{\psi}{2}, \quad (2)$$

and the unit vector $\bar{\rho}_0$ in the ρ direction is

$$\bar{\rho}_0 = \bar{x}\cos\xi\sin\psi + \bar{y}\sin\xi\sin\psi - \bar{z}\cos\psi. \quad (3)$$

In general, the surface current induced on the paraboloid will have components K_x, K_y, and K_z. For high-gain reflectors having apertures many wavelengths in diameter, it is only the K_x and K_y components of current that contribute to the principal part of the diffraction pattern centered about the z axis. Therefore, component K_z will be neglected in the rest of the discussion.

Short Electric-Dipole Feed

For a short electric-dipole feed lying along x axis, of height dx, and excited with a current I flowing in $-x$ direction, the far-zone components of electric field are

$$\bar{E} = \frac{j\eta I dx\epsilon^{-jk\rho}}{2\lambda\rho}\left[\bar{x}(\cos^2\psi\cos^2\xi + \sin^2\xi) - \bar{y}\frac{\sin 2\xi\sin^2\psi}{2} + \bar{z}\frac{\sin 2\psi\cos\xi}{2}\right]. \quad (4)$$

The substitution of (2), (3), and (4) into (1) yields

$$\bar{K} = \frac{jIdx\epsilon^{-jk\rho}}{\lambda\rho}\cos\frac{\psi}{2}\left[\bar{x}(\cos\psi + \sin^2\xi(1-\cos\psi) - \frac{\bar{y}}{2}\sin 2\xi(1-\cos\psi)\right]. \quad (5)$$

The projected electric field in the aperture is given as

$$-\frac{\bar{K}\eta}{2\cos\frac{\psi}{2}}.^{1}$$

Making this substitution it is found that[2]

$$\bar{E}_a = -\frac{j\eta I dx\epsilon^{-jk(f+z_0)}}{4\lambda\rho}\{\bar{x}[(1+\cos\psi) - (1-\cos\psi)\cos 2\xi] - \bar{y}\sin 2\xi(1-\cos\psi)\}. \quad (6)$$

It is seen that the aperture electric field has a unidirectional component along the x axis as well as a cross-polarized component parallel to the y axis. The cross-polarized component has the interesting symmetry property, in that it is oppositely directed in adjacent quadrants.

Fig. 2 shows the distribution of electric field in the aperture of a paraboloid reflector with an electric-dipole feed, together with characteristics of the patterns arising from such a distribution. It is seen that the principal polarization patterns measured in the E and H planes have the customary shape with their maxima on the polar axis. On the other hand, the cross-polarized lobes (which are often called Condon lobes) measured, in the planes at 45 degrees to the principal planes where the cross-polarization is a maximum, have minimum intensity on the polar axis and maximum intensity off axis. The position of maximum intensity corresponds approximately to the position of the first null in the principal polarization patterns. Because these cross-polarized lobes often have a magnitude considerably higher than the first side lobe of the principal polarization patterns, they can be troublesome in a radar application in which the target reflects energy polarized at right angles to that incident upon it.

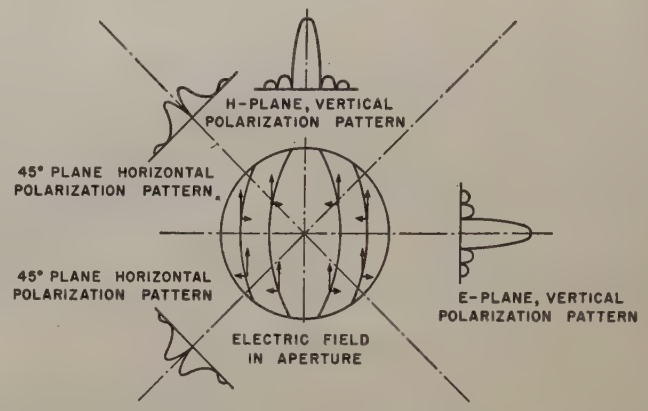

Fig. 2—Electric field in the paraboloid reflector aperture and resulting far-zone radiation patterns when the paraboloid is excited by a vertically oriented electric dipole.

Short Magnetic-Dipole Feed

For a short magnetic dipole lying along the y axis with a length dy and excited with a magnetic current M flowing in the $+y$ direction, the far-zone components of electric field are

$$\bar{E} = \frac{jMdy\epsilon^{-jk\rho}}{2\lambda\rho}[\bar{x}\cos\psi + \bar{z}\sin\psi\cos\xi]. \quad (7)$$

Following the procedure outlined above, the projected field in the aperture is

$$\bar{E}_a = -\frac{jMdy\epsilon^{-jk(f+z_0)}}{4\lambda\rho}\{\bar{x}[(1+\cos\psi) + (1-\cos\psi)\cos 2\xi] + \bar{y}[\sin 2\xi(1-\cos\psi)]\}. \quad (8)$$

Here again it is seen that the aperture electric field has a unidirectional component along the x axis but the cross-polarized component of electric field is oppositely directed. Fig. 3 shows a sketch of the aperture field.

Plane-Wave Feed

If the paraboloid could be excited by a combination of electric and magnetic dipoles, oriented at right angles to one another and having the proper values of electric and

[1] S. Silver, "Microwave Antenna Theory and Design," McGraw-Hill Book Co., New York, N. Y., p. 417; 1949.
[2] E. U. Condon, "Theory of Radiation from Paraboloid Reflectors," Westinghouse Research Report SR-105; September, 1941.

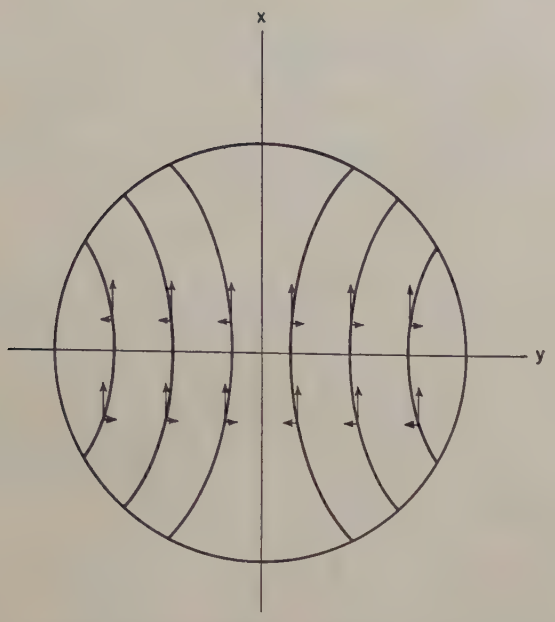

Fig. 3—Electric field in paraboloid reflector aperture when paraboloid is excited by a short magnetic dipole lying along y axis.

magnetic current, it is seen that the y directed component of the aperture field could be made to disappear. The proper value of the ratio of the magnetic to electric current is η which is the same as the ratio of the equivalent magnetic and electric current densities in a plane-wave source. The aperture field, $\bar{E}_a$, of a paraboloid excited by a plane wave-source with electric field intensity E_x and dimensions dx and dy small compared to a wavelength, is then seen to be from (6) and (8)

$$\bar{E}_a = -\bar{x}j\frac{E_x dx dy}{\lambda\rho}\frac{(1+\cos\psi)}{2}\epsilon^{-jk(f+z_0)}. \qquad (9)$$

A sketch of this aperture field is shown in Fig. 4.

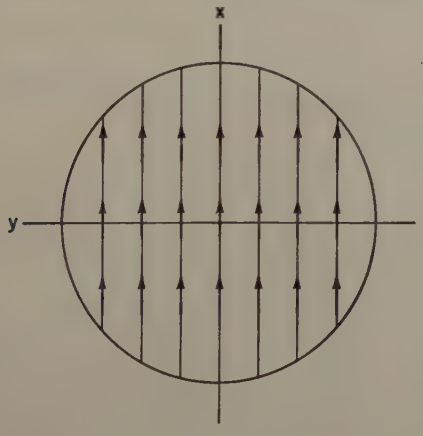

Fig. 4—Electric field in paraboloid reflector aperture when paraboloid is excited by a small plane-wave source polarized along x axis.

Hyperboloid Lens Aperture Distributions

Fig. 5 shows a sketch of the hyperboloid lens illustrating the notation used in the analysis. The aperture field of the hyperboloid lens of refractive index n is determined, subject to the conditions outlined previously, in a slightly different manner than the aperture field of the paraboloid reflector. First, the field incident on the lens from the feed is resolved into a component in the plane of incidence and one perpendicular to it. The amount of each of these components transmitted into the lens through surface 1 is then computed from the plane-wave boundary conditions at the dielectric-air interface, which are summarized in Fresnel's equations. Finally, the amount of energy transmitted through surface 2 is computed. The assumption is made, in deriving this aperture field, that the multiple transits of energy in the lens between the two surfaces are unimportant. These transits can be neglected because they give rise to small amplitude and phase variations arranged in concentric rings in the aperture, superimposed on the constant phase amplitude distribution produced by the single transit. In any lens of reasonable size they produce small amplitude diffraction patterns, split off at wide angles from the polar axis.[3,4]

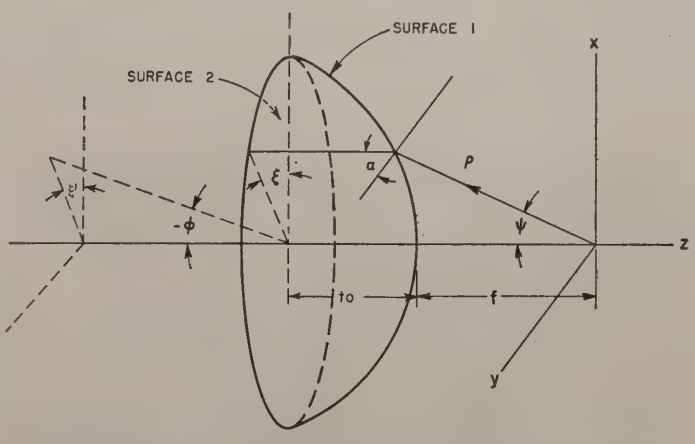

Fig. 5—Sketch of the hyperboloid lens illustrating the notation used in the analysis.

Electric-Dipole Feed

When the hyperboloid lens is excited by an electric dipole lying along the x axis, of length dx, excited by a current I following in the $-x$ direction, the electric field incident on the curved surface of the lens is

$$\bar{E} = j\frac{\eta I dx\epsilon^{-jk\rho}}{2\lambda\rho}\left[\bar{\psi}\cos\xi\cos\psi - \bar{\xi}\sin\xi\right] \qquad (10)$$

where the $\bar{\psi}$ component lies in the plane of incidence, and the $\bar{\xi}$ component lies perpendicular to the plane of incidence. The electric field transmission coefficient, $T_\parallel$, for the field polarized in the plane of incidence is

$$T_\parallel = \frac{2\cos(\psi+\alpha)\sin\alpha}{\sin(\psi+2\alpha)\cos\psi}, \qquad (11)$$

[3] J. Brown, "Effect of amplitude variations in aperture fields on side lobes," *Jour. Inst. Elect. Eng.*, vol. 97, part III, pp. 419–424; November, 1950.

[4] N. I. Korman, E. B. Herman, and I. R. Ford, "Analysis of microwave antenna side-lobes," *RCA Review*, vol. 13, pp. 323–334; September, 1952.

while the electric field transmission coefficient for the $T_\perp$ component of field, polarized perpendicular to the plane of incidence is

$$T_\perp = \frac{2\cos(\psi+\alpha)\sin\alpha}{\sin(\psi+2\alpha)}. \tag{12}$$

The transmitted electric field lying in the plane of incidence becomes

$$E_\parallel = j\frac{\eta I dx}{\lambda\rho}\epsilon^{-jk\rho}\left[\frac{\cos(\psi+\alpha)\sin\alpha\cos\xi}{\sin(\psi+\alpha)}\right], \tag{13}$$

while the transmitted field lying perpendicular to the plane of incidence becomes

$$E_\perp = -j\frac{\eta I dx\epsilon^{-jk\rho}}{\lambda\rho}\left[\frac{\cos(\psi+\alpha)\sin\alpha\sin\xi}{\sin(\psi+\alpha)}\right]. \tag{14}$$

After refraction at the curved surface of the lens, there will be no ϵ_z field. The ϵ_x- and ϵ_y-components of the field will be

$$\epsilon_x = E_\parallel\cos\xi - E_\perp\sin\xi, \tag{15}$$

and

$$\epsilon_y = E_\parallel\sin\xi + E_\perp\cos\xi.$$

These transverse components of field will all arrive in phase at the aperture after traveling their respective distances through the lens. The value of electric field just outside the dielectric will be

$$E_a = \bar{x}\frac{2j\eta I dx\epsilon^{-jk(f+nt_0)}}{\lambda\rho}\left[\frac{n}{(n+1)}\frac{\cos(\psi+\alpha)\sin\alpha}{\sin(\psi+2\alpha)}\right]. \tag{16}$$

Thus the hyperboloid lens excited by an electric dipole has no cross-polarized components of aperture field.

Magnetic-Dipole Feed

When the hyperboloid lens is excited by a magnetic dipole lying along the y axis with a length dy and excited by a magnetic current M flowing in the $+y$ direction, the field incident on the curved surface of lens becomes

$$\bar{E} = \frac{jMdy\epsilon^{-jk\rho}}{2\lambda\rho}[\bar{\psi}\cos\xi - \bar{\xi}\sin\xi\cos\psi]. \tag{17}$$

Tracing the field through the lens as before, now the aperture field has both a principal and transverse polarization component. The aperture field is

$$\bar{E}_a = \frac{jMdy\epsilon^{-jk(f+nt_0)}}{\lambda\rho}\frac{n}{n+1}\frac{\cos(\psi+\alpha)\sin\alpha}{\sin(\psi+2\alpha)\cos\psi}$$
$$\cdot[\bar{x}(1+\cos^2\psi+\sin^2\psi\cos 2\xi)+\bar{y}(\sin 2\xi\sin^2\psi)]. \tag{18}$$

Plane-Wave Feed

The aperture field of the lens, when it is excited by a plane-wave source with electric field intensity E_x, can be obtained in the manner outlined previously. The aperture field is

$$\bar{E}_a = j\frac{E_x dxdy}{\lambda\rho}\frac{n}{(n+1)}\cdot\frac{\cos(\psi+\alpha)\sin\alpha}{\sin(\psi+2\alpha)\cos\psi}\epsilon^{-jk(f+nt_0)}$$
$$\cdot\{\bar{x}[(1+\cos\psi)^2+\sin^2\psi\cos 2\xi]+\bar{y}\sin^2\psi\sin 2\xi\}, \tag{19}$$

and it is seen that here too, there is both a principal and cross-polarized component of aperture field.

Far-Zone Diffraction Patterns

The integral expressions for the far-zone field components, E_ϕ and $\bar{E}_\xi$, of the foregoing aperture distributions, that have the ratio of tangential E to tangential H equal to the impedance of free space, can be set up in the standard fashion. For narrow radiated beams it is permissible to approximate the spherical co-ordinate far-zone fields by rectangular components E_x and E_y. The expressions for these components are

$$\bar{E} = j\frac{\epsilon^{-jkR}}{\lambda R}\left[\int_A \bar{E}_a\epsilon^{-jkr\sin\phi\cos(\xi-\xi')}rdrd\xi\right]. \tag{20}$$

Paraboloid Reflector with Electric-Dipole Feed

If the following substitutions are made in (6)

$$u = \frac{r}{2f}, \qquad \gamma = \frac{D}{4f},$$
$$F = \frac{j\eta I dx\epsilon^{-jk(f+z_0)}}{2\lambda},$$
$$\rho = \frac{2f}{1+\cos\psi}, \qquad \beta = 2kf\sin\phi,$$

the far-zone fields $\bar{E}$ of the paraboloid excited by an electric dipole become

$$\bar{E} = j\frac{\epsilon^{-jkR}}{\lambda R}4fF\int_0^{2\pi}\int_0^{\gamma}\left\{\bar{x}\left(-\frac{1}{(1+u^2)^2}+\frac{u^2\cos 2\xi}{(1+u^2)^2}\right)\right.$$
$$\left.+\bar{y}\left(\frac{u^2\sin 2\xi}{(1+u^2)^2}\right)\right\}\epsilon^{-j\beta u\cos(\xi-\xi')}ududu\xi. \tag{21}$$

Integration with respect to the angular variable ξ can be carried out since

$$\int_0^{2\pi}\epsilon^{j\beta u\cos(\xi-\xi')}\begin{Bmatrix}\cos n\xi\\ \sin n\xi\end{Bmatrix}d\xi = 2\pi(j)^n\begin{Bmatrix}\cos n\xi'\\ \sin n\xi'\end{Bmatrix}J_n(\beta u).$$

Performing this integration (21) becomes

$$\bar{E} = -j\frac{\epsilon^{-jkR}}{\lambda R}8\pi fF\int_0^{\gamma}\left\{\bar{x}\left(\frac{uJ_0(\beta u)}{(1+u^2)^2}+\frac{u^3J_2(\beta u)\cos 2\xi'}{(1+u^2)^2}\right)\right.$$
$$\left.+\bar{y}\frac{u^3J_2(\beta u)\sin 2\xi'}{(1+u^2)^2}\right\}du. \tag{22}$$

This integral cannot be evaluated exactly because of the presence of the term $1/(1+u^2)^2$. However, if this term is approximated by a polynomial as

$$\frac{1}{(1+u^2)^2} = a_0 + a_2u^2 + \cdots + a_{2n}u^{2n}, \tag{23}$$

these integrals can be evaluated in terms of tabulated

TABLE I

COMPUTED PATTERN CHARACTERISTICS AND GAIN FACTOR OF PARABOLOIDS EXCITED BY A SHORT ELECTRIC DIPOLE

D-Wave Lengths	f/D	H-Plane Half-Power Beam-Width (degrees)	E-Plane Half-Power Beam-Width (degrees)	Position of Cross-Polarization Maximum	H-Plane First Side-Lobe Level (db)	E-Plane First Side-Lobe Level (db)	Cross-Polarized Lobe Max. Level (db)	Gain Factor
37.2	0.25	1.6	2.2	1.8	−16.5	−36.5	−15.8	0.41
37.2	0.30	1.6	2.0	1.8	−16.5	−32	−18.1	0.37
37.2	0.40	1.6	1.75	1.8	−17.2	−24.7	−22.2	0.32
37.2	0.46	1.6	1.75	1.8	−17.2	−22.9	−24.3	0.28
37.2	0.60	1.6	1.75	1.8	−17.4	−20	−28	0.19

functions, since repeated integration by parts puts each term in the form

$$\int x^{p+1}J_p(x)dx = x^{p+1}J_{p+1}(x). \tag{23a}$$

The coefficients a_{2n} of (23) are chosen here so that the polynomial is the least square approximation to the desired function.[5] It has been found that retaining only the first three coefficients that have values of 0.9823, −1.468, and 0.7445 respectively, the difference between the desired and approximating function is less than .02.

Performing the above manipulations, it is found that the far-zone field is

$$\begin{aligned}\bar{E} = -j\frac{\epsilon^{-jkR}}{\lambda R}\,8\pi fF\Bigg\{\bar{x}\Bigg[&(a_0\gamma^2 + a_2\gamma^4 + a_4\gamma^6)\frac{J_1(\beta\gamma)}{\beta\gamma} \\ &- 2(a_2\gamma^4 + 2a_4\gamma^6)\frac{J_2(\beta\gamma)}{(\beta\gamma)^2} + 8a_4\gamma^6\frac{J_3(\beta\gamma)}{(\beta\gamma)^3}\Bigg] \\ &+ \bar{x}\cos 2\xi'\Bigg[(a_0\beta^2\gamma^6 + a_2\beta^2\gamma^8 + a_4\beta^2\gamma^{10})\frac{J_3(\beta\gamma)}{(\beta\gamma)^3} \\ &- 2\beta^2(a_2\gamma^8 + 2a_4\gamma^{10})\frac{J_4(\beta\gamma)}{(\beta\gamma)^4} + 8a_4\beta^2\gamma^{10}\frac{J_5(\beta\gamma)}{(\beta\gamma)^5}\Bigg] \\ &+ \bar{y}\beta^2\sin 2\xi'\Bigg[(a_0\gamma^6 + a_2\gamma^8 + a_4\gamma^{10})\frac{J_3(\beta\gamma)}{(\beta\gamma)^3} \\ &- 2(a_2\gamma^8 + 2a_4\gamma^{10})\frac{J_4(\beta\gamma)}{(\beta\gamma)^4} + 8a_4\gamma^{10}\frac{J_5(\beta\gamma)}{(\beta\gamma)^5}\Bigg]\Bigg\}\end{aligned} \tag{24}$$

Neglecting direct radiation from the feed, the maximum power gain of the paraboloid excited by an electric dipole can be computed as follows from the definition of power gain.

$$G = 4\pi\,\frac{\text{Power radiated per unit solid angle by the aperture}}{\text{Total power radiated by the feed}}$$

$$= \frac{4\pi}{\lambda^2}\left(\frac{\pi D^2}{4}\right)\left\{6\left[\frac{a_0\gamma}{2} + \frac{a_2\gamma^3}{4} + \frac{5}{12}a_4\gamma^5\right]^2\right\}. \tag{25}$$

The term in braces, $\{\ \}$, in (25) is often called the gain factor. It has a maximum value of unity for a uniformly illuminated aperture which has constant phase, and lesser values for all other amplitude distributions which have constant phase.

Diffraction patterns have been computed from (24) for a series of paraboloids with a 37.2 wavelength aperture diameter and various focal lengths. The gain factor for these reflectors has been computed from (25). A typical pattern is shown in Fig. 6 for one of these paraboloids which has an f/D ratio of 0.25. Pertinent data about this pattern and the other computed patterns are summarized in Table I above.

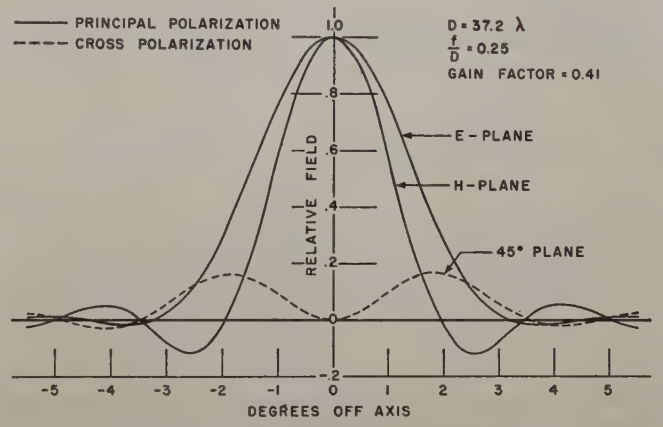

Fig. 6—Paraboloid diffraction patterns with electric dipole feed.

It is seen from Fig. 6, that when the feed lies in the aperture plane, the principal polarization pattern is wider in the E-plane than the H-plane and the side-lobe level is higher in the H-plane than the E-plane. This behavior is consistent with the fact that the aperture distribution is much more strongly tapered in the E-plane than the H-plane. The cross-polarized lobes measured in planes at 45 degrees to the principal planes, where they attain their maximum value, lie quite close to the polar axis and are higher than the first side lobes in either of the principal planes. The gain factor for this antenna, however, is only 0.41. Table I shows that paraboloids of the same aperture diameter but with longer focal lengths have similar H-plane patterns, but have E-plane patterns with narrower beam-widths and higher side-lobe levels. The cross-polarized lobes and gain factor, however, both decrease as the focal length increases.

[5] W. E. Milne, "Numerical Calculus," Princeton University Press, Princeton, N. J., chap. IX, 1949.

Paraboloid Reflector with Magnetic-Dipole Feed

The results for the paraboloid excited by a short electric dipole oriented along the x axis apply, with minor modifications, to a paraboloid excited by a short magnetic dipole lying along the y axis. Therefore, a detailed discussion will not be given here. However, the principal characteristics of a paraboloid excited by a magnetic dipole lying along the y axis are summarized below.

(1) The E-plane diffraction patterns of the paraboloid with magnetic-dipole feed correspond to the H-plane diffraction patterns of the paraboloid with electric-dipole feed.
(2) The H-plane diffraction patterns of the paraboloid with the magnetic-dipole feed correspond to the E-plane diffraction patterns of the paraboloid with electric-dipole feed.
(3) The cross-polarized patterns in both cases are the negative of one another.
(4) The gain of the two systems is the same.

Paraboloid Reflector with Plane-Wave Feed

When a paraboloid reflector is fed by a plane-wave feed with no variation of field intensity in the E-plane dimension B, and a half-sinusoidal variation in field intensity across the H-plane dimension A, the aperture field of the paraboloid becomes

$$\overline{E}_a = -\bar{x}j\frac{E_x AB(1+\cos\psi)^2}{2\pi\lambda f}\epsilon^{-jk(f+\rho_0)} \cdot \left[\frac{\sin\left(\frac{\pi B}{\lambda}\sin\psi\cos\xi\right)}{\frac{\pi B}{\lambda}\sin\psi\cos\xi}\cdot\frac{\cos\left(\frac{\pi A}{\lambda}\sin\psi\sin\xi\right)}{1-\left(\frac{2A}{\lambda}\sin\psi\sin\xi\right)^2}\right]. \quad (26)$$

If the dimension A, of the plane-wave feed is chosen to be about 1.42 B, the principal lobe of the E- and H-plane patterns of the feed are almost identical and the patterns in other planes are very similar. Using this approximation then, the paraboloid aperture field becomes

$$\overline{E}_a = -\bar{x}j\frac{E_x 1.42B^2(1+\cos\psi)^2}{2\pi\lambda f}\epsilon^{-jk(f+\rho_0)} \cdot \left[\frac{\sin\left(\frac{\pi B}{\lambda}\sin\psi\right)}{\frac{\pi B}{\lambda}\sin\psi}\right]. \quad (27)$$

Proceeding as in the case of the electric-dipole feed, it is easy to show that the far-zone field of the reflector with a plane-wave feed is

$$\overline{E} = \bar{x}\frac{E_x 5.68B^2\epsilon^{-jk(f+\rho_0+R)}}{\lambda^2 fR}\left[(b_0d^2+b_2d^4+b_4d^6)\frac{J_1(\beta d)}{\beta d} - 2(b_2d^4+2b_4d^6)\frac{J_2(\beta d)}{(\beta d)^2} + 8b_4d^6\frac{J_3(\beta d)}{(\beta d)^3}\right], \quad (28)$$

where $d=D/2$ and the coefficients b_0, b_2, and b_4 are the coefficients of the polynomial which approximates the aperture distribution normalized to a maximum value of unity.

It is noticed that the far-zone field has no cross-polarized radiation fields.

Similarly, the power gain of the reflector excited by the plane-wave source becomes

$$G = \left(\frac{4\pi}{\lambda^2}\right)\left(\frac{\pi D^2}{4}\right)\left\{\frac{45.4B^2}{\pi\lambda^2 f^2}\left[\frac{a_0 d}{2}+\frac{a_2 d^3}{4}+\frac{5}{12}a_4 d^5\right]^2\right\} \quad (29)$$

where, as before, the factor in the braces, $\{\ \}$, is the gain factor.

The diffraction pattern of a paraboloid with a 37.2 wavelength diameter aperture, and f/D ratio of 0.46, and an edge illumination of -12 db is shown in Fig. 7. The shape of this principal polarization pattern is rotationally symmetric about the polar axis because of the rotationally symmetric properties assumed for the feed pattern.

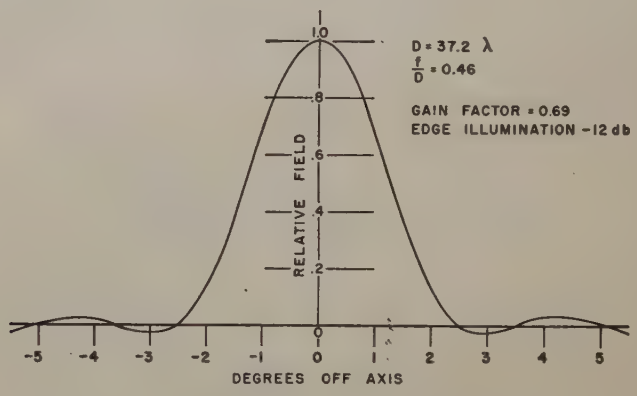

Fig. 7—Paraboloid diffraction pattern with plane-wave feed.

Diffraction patterns and gain factor of this paraboloid for various edge illuminations have been computed and are tabulated in Table II below.

TABLE II
PATTERN CHARACTERISTICS AND GAIN FACTOR OF A PARABOLOID EXCITED BY A PLANE-WAVE SOURCE
Aperture Diameter = 37.2 Wavelengths, $f/D = 0.46$

Edge Illumination (db)	Half-Power Beam-Width (degrees)	First Side-Lobe Level (db)	Gain Factor
−8	1.74	−23.7	0.53
−10	1.80	−26	0.66
−12	1.82	−29.1	0.69
−16	1.96	−37.1	0.67
−20	2.06	−46	0.61
−30	2.36	−36.5	0.51

As the edge illumination decreases from -8 db, the width of the main beam increases as is expected. On the other hand, the first side-lobe level initially decreases, reaching a minimum for an edge illumination of about -20 db, and then increases. The gain factor is low for

high edge illumination, where the aperture efficiency is high, but the spill-over loss is large. A maximum of gain is reached at an edge illumination of about −12 db. For still lower edge illuminations, the gain decreases because the aperture efficiency decreases.

Hyperboloid Lens with Plane-Wave Feed

The aperture field of a hyperboloid lens just outside the dielectric, fed by a plane-wave feed that has no variation of field intensity in the E-plane dimension B, and a half sinusoidal variation in field intensity across the H-plane dimension A, subject to the previous approximations, is

$$\bar{E}_a = j\frac{E_x 2.84B^2}{\pi\lambda f}\epsilon^{-jk(f+nt_0)} \cdot \left\{ \frac{n\sin\left(\frac{\pi B}{\lambda}\right)\sin\psi\tan\psi\cos^2(\psi+\alpha)}{(n^2-1)\frac{\pi B}{\lambda}\sin\psi\sin(\psi+2\alpha)} \cdot \bar{x}[(1+\cos\psi)^2+\sin^2\psi\cos 2\xi]+\bar{y}\sin^2\psi\sin 2\xi \right\}. \quad (30)$$

Eq. (29) can be written in terms of the approximating polynomials in r, the aperture radius, as

$$\bar{E}_a = j\frac{E_x 2.84B^2\epsilon^{-jk(f+nt_0)}}{\pi\lambda f}\{\bar{x}[f(r)+g(r)\cos 2\xi] + \bar{y}g(r)\sin 2\xi\}. \quad (31)$$

Proceeding as before, the far-zone field becomes

$$\bar{E} = -\frac{E_x 5.68B^2\epsilon^{-jk(f+nt_0+R)}}{\lambda^2 fR}\int_0^{d.}\{\bar{x}[f(r)J_0(\beta r) - g(r)J_2(\beta r)\cos 2\xi'] - \bar{y}g(r)J_2(\beta r)\sin 2\xi'\}rdr. \quad (32)$$

It is found that in order to have the polynomials $f(r)$ and $g(r)$ approximate this aperture distribution closely, they must contain terms in r as

$$c_0 + c_1 r + c_2 r^2 + c_3 r^3.$$

Eq. (32) can be evaluated in terms of tabulated functions, since integration by parts puts each term either in the form of (23a) or[6]

$$\int_0^z (ax)^n J_n(ax)dx = 2^{n-1}\sqrt{\pi}\,\Gamma(n+\tfrac{1}{2})z \cdot [J_{n+1}(az)S_n(az) - S_{n+1}(az)J_n(az)] + \frac{(az)^{n+1}J_n(az)}{(2n+1)a},$$

where $S_n(ax)$ is a Struve function.

[6] N. W. McLachlan and A. L. Meyers, "Integrals involving Bessel and Struve functions," *Phil. Mag.*, vol. 21, p. 437; February, 1936.

The power gain of the hyperboloid lens is computed in similar fashion to the computation of power gain of the paraboloid with plane-wave feed, in terms of the coefficients of the polynomial $f(r)$. The expressions for the diffraction field and power gain will not be written down since they are rather lengthy. However, some data obtained from these expressions will be presented. Fig. 8

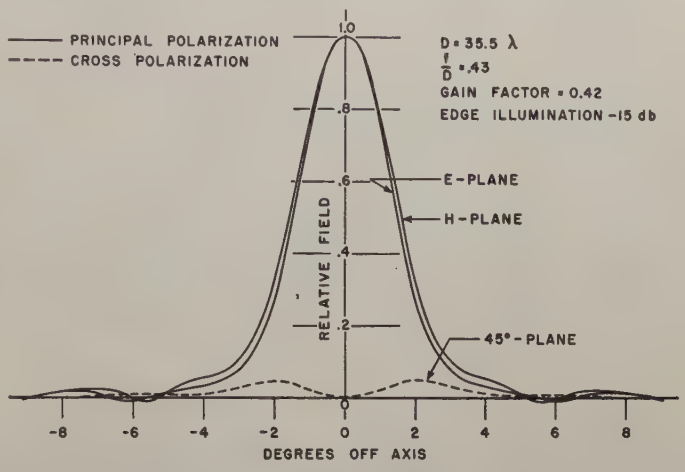

Fig. 8—Hyperboloid lens diffraction patterns with plane-wave feed.

shows the diffraction pattern of a hyperboloid lens, with a 35.5 wavelength diameter aperture, an f/D ratio of 0.41, and a refractive index of 1.57 excited by a plane-wave source to give a −15 db edge illumination at the curved surface of the lens. It is noticed that, although the illumination of the curved surface of the lens is symmetric about the polar axis, the E-plane pattern here is narrower than the H-plane pattern. The reason for this is because illumination in this plane is less tapered, since the transmission coefficient for the lens is greater in the E plane. The computed gain factor of the lens is a maximum for this edge illumination, at a value of 0.42, which is almost 2.2 db less than the 0.69 gain factor obtainable with the paraboloid of about the same f/D ratio. This decreased gain is due to the approximately 0.21 db reflection loss at each lens surface, coupled with the poor aperture efficiency and high spill-over loss of the lens. Table III, on the following page, summarizes the important pattern characteristics of the above lens and another lens, of refractive index 1.57 for various edge illuminations. This table shows that, for each of the lenses, the beam-widths in the principal planes are narrow for high-edge illumination, and wide for low-edge illumination. The gain factor, on the other hand, reaches a maximum for some intermediate illumination which represents the best compromise between high aperture efficiency and low spill-over loss. For each lens, the maximum level of the cross-polarized lobes decreases as the edge illumination is decreased, since the average amplitude of the cross-polarized aperture fields is less for low-edge illumination. The longer focal-length lens has lower cross-polarized lobes for a given edge illumination since it subtends a smaller angle at the feed point. The angular

TABLE III

COMPUTED PATTERN CHARACTERISTICS AND GAIN FACTOR OF TWO HYPERBOLOID LENSES EXCITED BY PLANE-WAVE SOURCES

D-Wave Lengths	f/D	Edge Illumination (db)	E-Plane Half-Power Beam Width (degrees)	H-Plane Half-Power Beam Width (degrees)	Max. Level of Cross-Polarization Lobe (db)	E-Plane First Side-Lobe Level (db)	H-Plane First Side-Lobe Level (db)	Gain Factor
35.5	0.43	−10	2.0	2.1	−31.4	−30.5	−28.4	0.35
35.5	0.43	−15	2.2	2.3	−32.0	−40	−46	0.42
35.5	0.43	−20	2.4	2.5	−32.8	−38	−34	0.38
35.5	0.43	−24	2.6	2.7	−34	−40	−30.5	0.31
35.5	0.77	−10	1.9	2.0	−38.7	−32.8	−40	0.53
35.5	0.77	−15	2.0	2.2	−39.2	−40	−45	0.53
35.5	0.77	−20	2.2	2.4	−40	−31.4	−40	0.47

position of the maximum of all the cross-polarized lobes for these lenses is about 2 degrees from the polar axis. There seems to be no systematic variation in the amplitude of the first side lobes in the principal plane patterns as edge illumination is varied, as there is in the case of the paraboloid reflector.

Experimental Results

Experimental radiation patterns and power gain measurements have been made at an operating frequency of 35,000 mc for a paraboloid reflector fed with a small rectangular horn, and for two hyperboloid dielectric lenses fed by small rectangular horns. The dimensions of the reflector and lenses used in these experiments correspond to those used in the above theoretical computations. The paraboloid reflector used is a searchlight reflector with a contour accuracy of better than a hundredth of a wavelength. The rectangular feed horn is connected to the signal source behind the reflector by means of a waveguide bent in the H plane through a total angle of 180 degrees in two 90 degree steps. Thus, there is a small amount of aperture blocking caused by this waveguide, which is not taken into account in the theory. The hyperboloid lenses are machined from polystyrene; their contour accuracy also being on the order of a hundredth of a wavelength.

An experimental radiation pattern of the paraboloid reflector excited by a pyramidal-horn feed, which gives an edge illumination of −20 db in the E plane and −21.5 db in the H plane, is shown in Fig. 9. Here it is noticed the cross-polarized lobes are −25 db. It has been found that the level of these lobes decreases monotonically as the H-plane dimension of the horn is increased. Because the wave impedance of the mode in the horn approaches 377 ohms (the impedance of free space) as this dimension is increased, this behavior tends to confirm the theory that a paraboloid excited by a plane-wave source with a wave impedance of 377 ohms would have no cross-polarized lobes at all. The level of the first side lobe in the E plane is −28 db, while that in the H plane is −33 db. The H-plane pattern has a half-power beam-width of 2.1 degrees; while the E-plane pattern has a half-power beam-width of 2.0 degrees because the aperture illumination is more strongly tapered in this plane. Reference to Table II shows that the experimental half-power beam-widths agree closely with the theoretical values, while the side lobe levels in the two cases are quite different.

Experimental radiation patterns of a hyperboloid lens, with an f/D ratio of 0.42, excited by a horn feed that gives an edge illumination of −24 db in the E and H planes, are shown in Fig. 10. It is noticed that the main beam is relatively quite broad, but the side lobes are very low, the highest one being −41 db. The cross-polarized lobes are −29 db, and lie close to the polar axis (compared to the width of the main beam). The

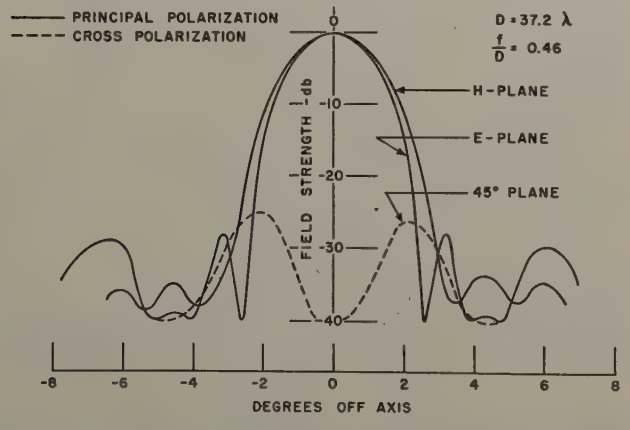

Fig. 9—Measured radiation patterns of a paraboloid reflector with a horn feed.

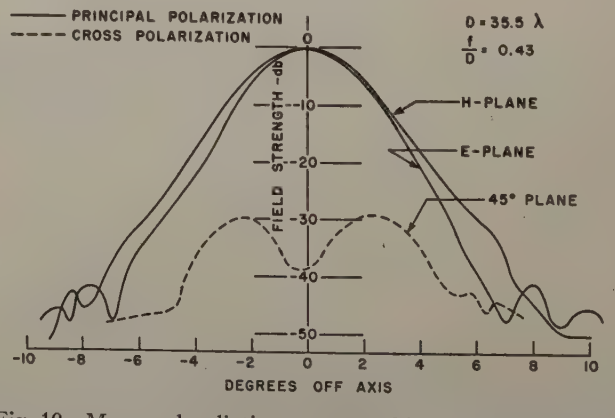

Fig. 10—Measured radiation patterns of hyperboloid lens with a horn feed.

TABLE IV

MEASURED PATTERN CHARACTERISTICS OF TWO HYPERBOLOID LENSES EXCITED BY PYRAMIDAL HORN FEEDS

D-Wave Lengths	*f/D*	Principal Plane Av. Illumination (db)	*E*-Plane Half-Power Beam-Width (degrees)	*H*-Plane Half-Power Beam-Width (degrees)	Max. Level of Cross-Polarization (db)	*E*-Plane First Side-Lobe Level (db)	*H*-Plane First Side-Lobe Level (db)	Gain Factor
35.5	0.42	−24	2.4	2.5	−29	−41	−42	0.26 ±0.013
35.5	0.77	−10	1.90	1.95	−28.5	−24.5	−27	0.42 ±0.021
35.5	0.77	−15	2.0	2.05	−31	−30	−30	0.41 ±0.021
35.5	0.77	−20	2.05	2.1	−35	−31.5	−31	0.390 ±0.020

measured gain factor of this lens is 0.26 which is low but consistent with the broad main beam. It is expected that the measured gain of the lenses should be about 8 per cent lower than the theoretical because the measured aperture efficiency of the experimental feed horns are only 75 per cent while the aperture efficiency of the plane-wave feeds used in the theoretical computation is 81 per cent. Allowing for this difference though, the experimental gain is still about 10 per cent less than theoretical. The additional discrepancy is probably accountable to absorption loss in the lens, and experimental error.

In Table IV, above, are summarized the results of measurements on the two hyperbolic lenses for various edge illuminations.

Comparison of the experimental measurements shown in Table IV with the theoretical results of Table III, for the lens with $f/D=0.77$, shows that the theory predicts the correct trend of the experimental results. The beamwidth of the experimental patterns is always narrower in the *E* plane than the *H* plane, and the principal plane beamwidths increase with decreasing edge illumination. However, the experimental beamwidths seem always to be narrower than theoretical. The measured gain factor is consistently about 20 per cent less than theoretical. The variation in amplitude of the measured cross-polarization lobes varies in the predicted fashion with edge illumination; however, the lobe values are always higher than theoretical. The measured side-lobe level in the principal planes, however, always decreases with decreasing-edge illumination.

CONCLUSION

It has been shown that low cross-polarized radiation lobes can be obtained from paraboloid reflectors when they are excited by small horns which approximate plane-wave sources. Low principal-polarization side lobes and low cross-polarized lobes can be obtained with a hyperboloid lens excited by a small horn, but the main beam is wide and the aperture efficiency is less than for paraboloids.

ACKNOWLEDGMENT

The work reported in this paper was sponsored by the Signal Corps Engineering Laboratory, Fort Monmouth, New Jersey.

INSTITUTIONAL LISTINGS

The IRE Professional Group on Antennas and Propagation is grateful for the assistance given by the firms listed below, and invites application for Institutional Listing from other firms interested in the field of Antennas and Propagation.

THE GABRIEL LABORATORIES, Div. of the Gabriel Co., 135 Crescent Road, Needham Heights 94, Mass.
Research and Development of Antenna Equipment for Government and Industry.

HUGHES AIRCRAFT COMPANY, Culver City, California
Research, Development, Manufacture: Radar, Guided Missiles, Tubes, Systems, Solid State Physics, Computers.

MARYLAND ELECTRONIC MANUFACTURING CORPORATION, College Park, Maryland
Antenna and System Development and Production for Civil and Military Requirements.

I-T-E CIRCUIT BREAKER CO., Special Products Div., 601 E. Erie Ave., Philadelphia 34, Pa.
Design, Development and Manufacture of Antennas and Related Equipment.

JANSKY & BAILEY, INC., 1339 Wisconsin Ave. N.W., Washington 7, D.C.
Radio & Electronic Engineering; Antenna Research & Propagation Measurements; Systems Design & Evaluation.

WHEELER LABORATORIES, INC., 122 Cutter Mill Road, Great Neck, New York
Consulting Services, Research and Development, Microwave Antennas and Waveguide Components.

The charge for an Institutional Listing is $25.00 per issue or $75.00 for four consecutive issues. Application for listing may be made to the Technical Secretary, The Institute of Radio Engineers, 1 East 79th Street, New York 21, New York.